Defense Nuclear Agency
Alexandria, VA 22310-3398

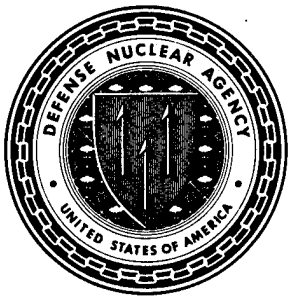

DNA-TR-94-150

Calculations to Support the Design of a Seismic Source Test

David M. O'Donnell
Michael W. McKay
Science Applications Intl Corp
10260 Campus Point Drive
San Diego, CA 92121-1578

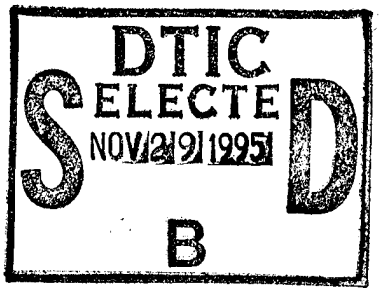

November 1995

Technical Report

CONTRACT No. DNA 001-93-C-0037

Approved for public release;
distribution is unlimited.

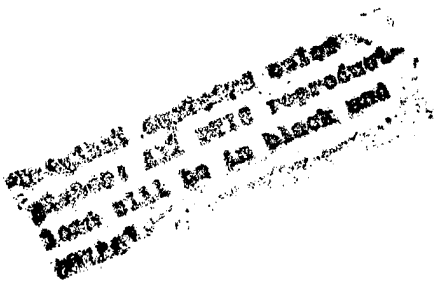

19951128 053

DTIC QUALITY INSPECTED 5

Destroy this report when it is no longer needed. Do not return to sender.

PLEASE NOTIFY THE DEFENSE NUCLEAR AGENCY, ATTN: CSTI, 6801 TELEGRAPH ROAD, ALEXANDRIA, VA 22310-3398, IF YOUR ADDRESS IS INCORRECT, IF YOU WISH IT DELETED FROM THE DISTRIBUTION LIST, OR IF THE ADDRESSEE IS NO LONGER EMPLOYED BY YOUR ORGANIZATION.

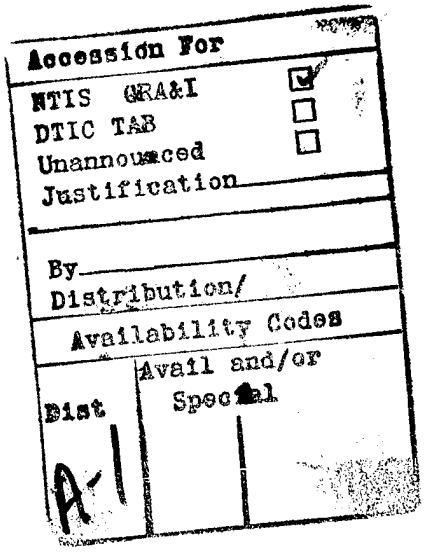

DISCLAIMER NOTICE

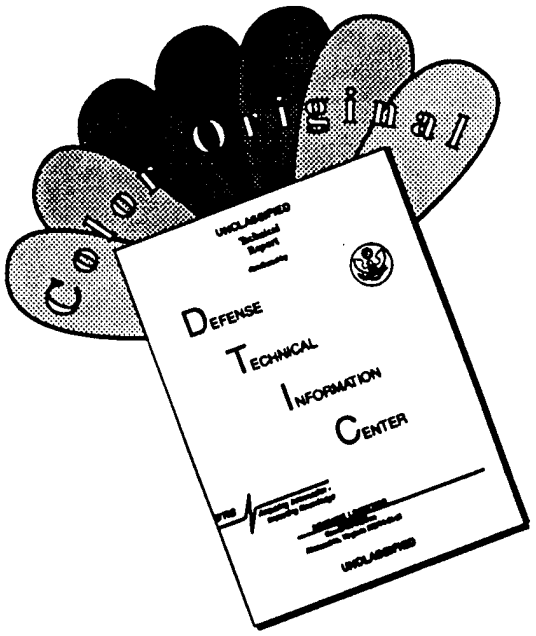

THIS DOCUMENT IS BEST QUALITY AVAILABLE. THE COPY FURNISHED TO DTIC CONTAINED A SIGNIFICANT NUMBER OF COLOR PAGES WHICH DO NOT REPRODUCE LEGIBLY ON BLACK AND WHITE MICROFICHE.

DISTRIBUTION LIST UPDATE

This mailer is provided to enable DNA to maintain current distribution lists for reports. (We would appreciate your providing the requested information.)

☐ Add the individual listed to your distribution list.

☐ Delete the cited organization/individual.

☐ Change of address.

NOTE:
Please return the mailing label from the document so that any additions, changes, corrections or deletions can be made easily. For distribution cancellation or more information call DNA/IMAS (703) 325-1036.

NAME: _____

ORGANIZATION: _____

OLD ADDRESS	CURRENT ADDRESS
_____	_____
_____	_____
_____	_____

TELEPHONE NUMBER: ( ) _____

DNA PUBLICATION NUMBER/TITLE	CHANGES/DELETIONS/ADDITIONS, etc.) *(Attach Sheet if more Space is Required)*
_____	_____
_____	_____
_____	_____

DNA OR OTHER GOVERNMENT CONTRACT NUMBER: _____

CERTIFICATION OF NEED-TO-KNOW BY GOVERNMENT SPONSOR (if other than DNA):

SPONSORING ORGANIZATION: _____

CONTRACTING OFFICER OR REPRESENTATIVE: _____

SIGNATURE: _____

CUT HERE AND RETURN

DEFENSE NUCLEAR AGENCY
ATTN: IMAS
6801 TELEGRAPH ROAD
ALEXANDRIA, VA 22310-3398

DEFENSE NUCLEAR AGENCY
ATTN: IMAS
6801 TELEGRAPH ROAD
ALEXANDRIA, VA 22310-3398

REPORT DOCUMENTATION PAGE

Form Approved OMB No. 0704-0188

Public reporting burden for this collection of information is estimated to average 1 hour per response, including the time for reviewing instructions, searching existing data sources, gathering and maintaining the data needed, and completing and reviewing the collection of information. Send comments regarding this burden estimate or any other aspect of this collection of information, including suggestions for reducing this burden, to Washington Headquarters Services, Directorate for Information Operations and Reports, 1215 Jefferson Davis Highway, Suite 1204, Arlington, VA 22202-4302, and to the Office of Management and Budget, Paperwork Reduction Project (0704-0188), Washington, DC 20503.

1. AGENCY USE ONLY (Leave blank)	2. REPORT DATE	3. REPORT TYPE AND DATES COVERED
	951101	Technical 930901 – 940630

4. TITLE AND SUBTITLE

Calculations to Support the Design of a Seismic Source Test

5. FUNDING NUMBERS

C - DNA 001-93-C-0037
PE - 62715H
PR - CD
TA - CD
WU - DH600180

6. AUTHOR(S)

David M. O'Donnell and Michael W. McKay

7. PERFORMING ORGANIZATION NAME(S) AND ADDRESS(ES)

Science Applications Intl Corp
10260 Campus Point Drive
San Diego, CA 92121-1578

8. PERFORMING ORGANIZATION REPORT NUMBER

SAIC-94/6909

9. SPONSORING/MONITORING AGENCY NAME(S) AND ADDRESS(ES)

Defense Nuclear Agency
6801 Telegraph Road
Alexandria, VA 22310-3398
FCTT/Ristvet

10. SPONSORING/MONITORING AGENCY REPORT NUMBER

DNA-TR-94-150

11. SUPPLEMENTARY NOTES

This work was sponsored by the Defense Nuclear Agency under RDT&E RMC Code T4613D CD CD 60018 5900A 25904D.

12a. DISTRIBUTION/AVAILABILITY STATEMENT

Approval for public release; distribution is unlimited.

12b. DISTRIBUTION CODE

13. ABSTRACT *(Maximum 200 words)*

Two numerical simulations were performed with the 2-D RAGE code to examine potential designs for a proposed seismic source test. The first calculation simulated the original design of the proposed SHIST test which was intended to demonstrate the use of near-source instrumentation developed in the HYDROPLUS program along with near-field seismic instrumentation to evaluate the seismic source function for hard rock. The calculation modeled the explosion of a 20-ton sphere of QM-100R explosive buried at a depth of approximately 40 meters. The second calculation was intended to examine whether the next test in the DISTANT MOUNTAIN test series, DM4, could also be used to satisfy some of the objectives of the SHIST test. For that calculation, the 20-ton charge (nitromethane in this case) was placed at the ground surface in a planar array typical of the DISTANT MOUNTAIN test series. An approximate yield equivalency factor for the two charge configurations was developed from the calculations.

14. SUBJECT TERMS			15. NUMBER OF PAGES
Ground Shock Seismic Source	SHIST DISTANT MOUNTAIN	RAGE Numerical Calculations	58 16. PRICE CODE

17. SECURITY CLASSIFICATION OF REPORT	18. SECURITY CLASSIFICATION OF THIS PAGE	19. SECURITY CLASSIFICATION OF ABSTRACT	20. LIMITATION OF ABSTRACT
UNCLASSIFIED	UNCLASSIFIED	UNCLASSIFIED	SAR

CLASSIFIED BY:

N/A since Unclassified.

DECLASSIFY ON:

N/A since Unclassified.

CONVERSION TABLE

Conversion Factors for U.S. Customary to Metric (SI) Units of Measurement

MULTIPLY → TO GET	BY	← DIVIDE
angstrom	1.000 000 X E-10	meters (m)
atmosphere (normal)	1.013 25 X E +2	kilo pascal (kPa)
bar	1.000 000 X E +2	kilo pascal (kPa)
barn	1.000 000 X E -28	meter^2 (m^2)
British thermal unit (thermochemical)	1.054 350 X E +3	joule (J)
calorie (thermochemical)	4.184 000	joule (J)
cal (thermochemical)/cm^2	4.184 000 X E -2	mega joule/m^2 (MJ/m^2)
curie	3.700 000 X E +1	*giga becquerel (GBq)
degree (angle)	1.745 329 X E -2	radian (rad)
degree Fahrenheit	$t_k = (t^\circ f+459.67)/1.8$	degree kelvin (K)
electron volt	1.602 19 X E -19	joule (J)
erg	1.000 000 X E -7	joule (J)
erg/second	1.000 000 X E -7	watt (W)
foot	3.048 000 X E -1	meter (m)
foot-pound-force	1.355 8818	joule (J)
gallon (U.S. liquid)	3.785 412 X E -3	meter^3 (m^3)
inch	2.540 000 X E -2	meter (m)
jerk	1.000 000 X E +9	joule (J)
joule/kilogram (J/kg) (radiation dose absorbed)	1.000 000	Gray (Gy)
kilotons	4.183	terajoules
kip (1000 lbf)	4.448 222 X E +3	newton (N)
kip/inch^2 (ksi)	6.894 757 X E +3	kilo pascal (kPa)
ktap	1.000 000 X E +2	newton-second/m^2 ($N-s/m^2$)
micron	1.000 000 X E -6	meter (m)
mil	2.540 000 X E -5	meter (m)
mile (international)	1.609 344 X E +3	meter (m)
ounce	2.834 952 X E -2	kilogram (kg)
pound-force (lbs avoirdupois)	4.448 222	newton (N)
pound-force inch	1.129 848 X E -1	newton-meter (N - m)
pound-force/inch	1.751 268 X E +2	newton/meter (N/m)
pound-force/foot^2	4.788 026 X E -2	kilo pascal (kPa)
pound-force/inch^2(psi)	6.894 757	kilo pascal (kPa)
pound-mass (lbm avoirdupois)	4.535 924 X E -1	kilogram (kg)
pound-mass-foot^2 (moment of inertia)	4.214 011 X E -2	kilogram-meter^2 ($kg - m^2$)
pound-mass-foot^3	1.601 846 X E +1	kilogram/meter^3 (kg/m^3)
rad (radiation dose absorbed)	1.000 000 X E -2	**Gray (Gy)
roentgen	2.579 760 X E -4	coulomb/kilogram (C/kg)
shake	1.000 000 X E -8	second (s)
slug	1.459 390 X E +1	kilogram (kg)
torr (mmHg, 0° C)	1.333 22 X E -1	kilo pascal (kPa)

* The becquerel (Bq) is the SI unit of radioactivity; 1 Bq = 1 event/s.
** The Gray (Gy) is the SI unit of absorbed radiation.

TABLE OF CONTENTS

FIGURES

FIGURES

SECTION 1
INTRODUCTION

This report presents the results of two numerical simulations performed by Science Application International Corporation (SAIC) for the Defense Nuclear Agency (DNA) to examine two potential designs for a proposed seismic source test. The purpose of the proposed test is to demonstrate the use of near-source instrumentation such as that used in the HYDROPLUS Program (Roessler and Killian, 1993; Cooper and Biwer, 1993) along with near-field seismic instrumentation to evaluate the seismic source function for hardrock. The name given to the proposed test is Seismic Hardrock In-situ Source Test (SHIST). The first of the two calculations presented here simulated the original design of the proposed SHIST experiment. i.e., it modeled the explosion of a 20-ton spherical charge of QM-100R explosive buried at a depth of approximately 40 meters. For the second calculation, the 20-ton charge was placed at the surface in a planar configuration similar to that used in the DISTANT MOUNTAIN test series* (Rocco, et al., 1993). The object of this calculation was to determine if the next test in the DISTANT MOUNTAIN test series, DM4, could also satisfy some of the objectives of the SHIST test. This configuration will be referred to in this report as SHIST/DM4. More details on the two test configuations and the results of the numerical simultions are provided in this report.

* The objective of the DISTANT MOUNTAIN test series was to evaluate borehole inclusion effects for HYDROPLUS gauges in hard rock.

SECTION 2
DESCRIPTION OF THE CALCULATIONS

2.1 COMPUTATIONAL METHOD.

The 2-D RAGE hydrocode was used in the SHIST and SHIST/DM4 simulations. RAGE is a 1-D, 2-D, and 3-D, AMR† Eularian hydrocode (Allen, et al., 1993; McKay, et al, 1993). The AMR technique, which utilizes an unstructured grid with square cells that automatically subdivides to any arbitrary level, places fine zoning where it is needed for accuracy while minimizing zoning in other regions. It utilizes this AMR technique along with a high-order Gonunov differencing scheme to achieve high accuracy. The code includes implicit, non-equilibrium grey radiation diffusion to calculate high-temperature hydrodynamic phenomena and also includes an elastic-plastic model to calculate material strength effects at lower pressures and temperatures. For the calculations described here, the radiation diffusion model was not required. The code also has an explosive detonation model using the JWL equation of state which was used in these simulations to model the high-explosive source.

The code also has fairly sophisticated output and post-processing capabilites for visualizing and analyzing the resulst of the calculations. Variables interpolated from the computational mesh are saved periodically at locations defined by a regularly spaced, structured, overlying mesh that is fixed for the duration of the calculation. This overlying mesh is necessary because of the transient nature of the computational mesh using the AMR method. The saved variables include the important physical variables such as pressure, material velocity, density, temperature, etc., at various times as well as peak values at each overlying mesh location for the duration for the calculation. This information is used for various graphic displays of the computatonal results including animations of, for instance, contour plots that show the time evolution of the solution. Several such contour plots are provided in Section 3 of this report.

The code also includes the capability to use massless Lagrangian tracer particles placed at specified locations throughout the computational domain for purposes of recording histories of the important variables. These tracer particles might represent gauges measuring material response variables (i.e., stress, particle velocity, or shock time-of-arrival gauges), or they may just be used to provide information for analyzing the results of the calculation. For the calculations being presented here, more than 100 tracer particles were placed within the grid to represent material-response gauges proposed for the tests and to record variable histories for other analysis purposes.

---

† Adaptive Mesh Refinement

2.2 COMPUTATIONAL CONFIGURATIONS.

The SHIST and SHIST/DM4 computational configurations are shown in Figures 2-1 and 2-2 respectively. The geology of the test bed consists of three horizontal layers of granite that increase in stiffness* with increasing depth. The depth intervals of the layers and their sound speeds is provided in Table 2-1 (Martinez, 1993).

Table 2-1. Depths and sound speeds of the three granite layers modeled for the proposed SHIST test site.

Layer Descriptor	Depth Interval (m)	Sound Speed (m/s)
Slow Granite	0 - 5	1200
Medium Granite	5 - 16	2200
Fast Granite	< 16	3400

In addition to these horizontal layers, the test site had a fault that intersected the surface at 85-m radius from the surface ground-zero and dipped at a 70° angle from the surface. This fault was not included in these calculations. We were prepared to continue the SHIST calculation as a 3-D calculation including the fault, but the stresses attenuated below the level of interest before the wave reached the fault zone.

Figure 2-1 shows the 3-m diameter spherical source consisting of 20 tons of QM-100R explosive buried at a depth of 39.6 meters. The 3.75-m diameter implacement hole was stemmed with DISTANT MOUNTAIN (DM) grout† (Rocco, et al., 1993) to a distance of approximately 6 meters from the center of the source. The stemming was completed with crushed-rock backfill to the surface. The axis of symetry for the 2-D cylindrical geometry used in the calculation was the center-line of the implacement hole.

The proposed instrumentation holes (gauge lines) are also shown in Figure 2-1. In our simulations, massless Lagrangain tracer particles were placed along these lines every 5 meters to a depth of 50 meters. These tracer particles allowed the recording of stress, particle velocity, and displacement as a function of time. The gauge lines shown for the SHIST calculation

---

* The layers were modeled with increasing stiffness consistent with the increasing sound speed that was measured at the proposed test site.

† DM grout is a high-density rock matching grout that was also used to stem HYDROPLUS gauge holes on the BEXAR event.

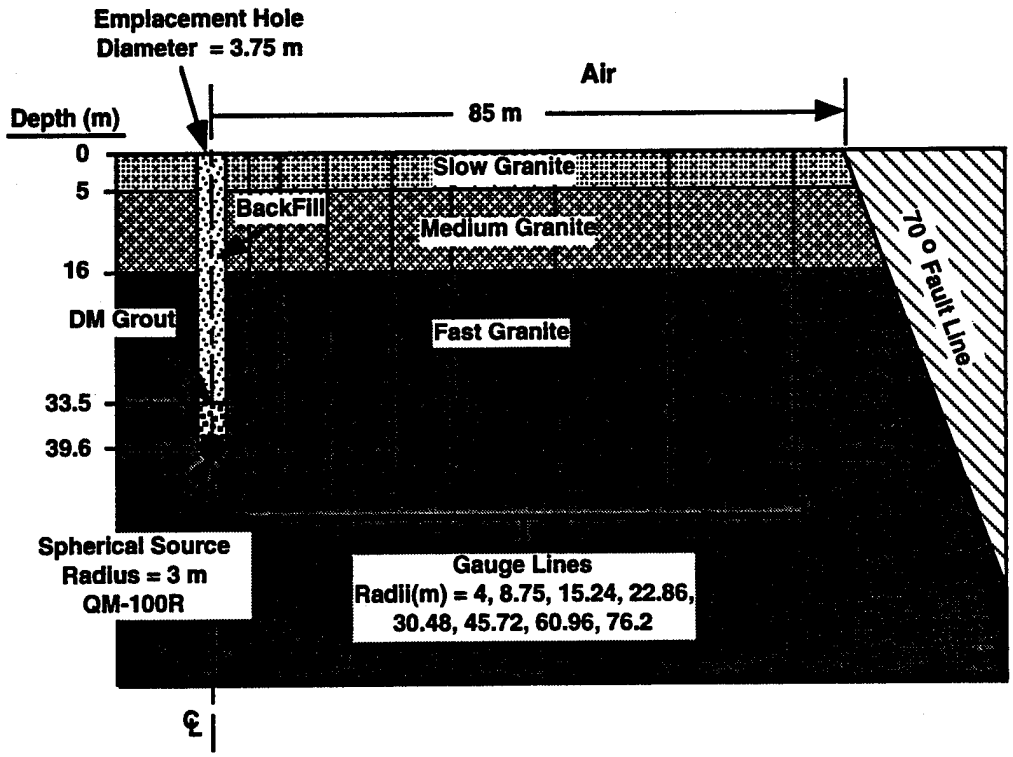

Figure 2-1. SHIST configuration.

(Figure 2-1) also apply to the SHIST/DM4 calculation; however, additional gauges (tracer particles) were located within the SHIST/DM4's granite slab.

The SHIST/DM4 simulation placed the HE near the surface as shown in Figure 2-2. A cylindrical pool, 6 meters in diameter and 0.62 meter deep, was filled with 20 tons of nitromethane (NM). The explosive was detonated simultaneously along the top surface. Directly below the NM was a hard granite slab ("fast granite" with zero porosity), 1.1 meters thick. This slab represents the DM4 test structure. Details of that test structure were not included. The actual experiment would place gauges in varous configurations within the granite slab in order to evaluate borehole inclusion effects in hard rock. In our simulation, we were only interested in the free-field shock propagated through the slab. Therefore, details of the DM4 gauges we omitted but several tracer particles were placed within the slab to monitor shock propogation. To increase coupling of the explosion to the ground, a 0.62-m thick berm of DM grout (for computational convenience) was placed over the nitromethane pool.

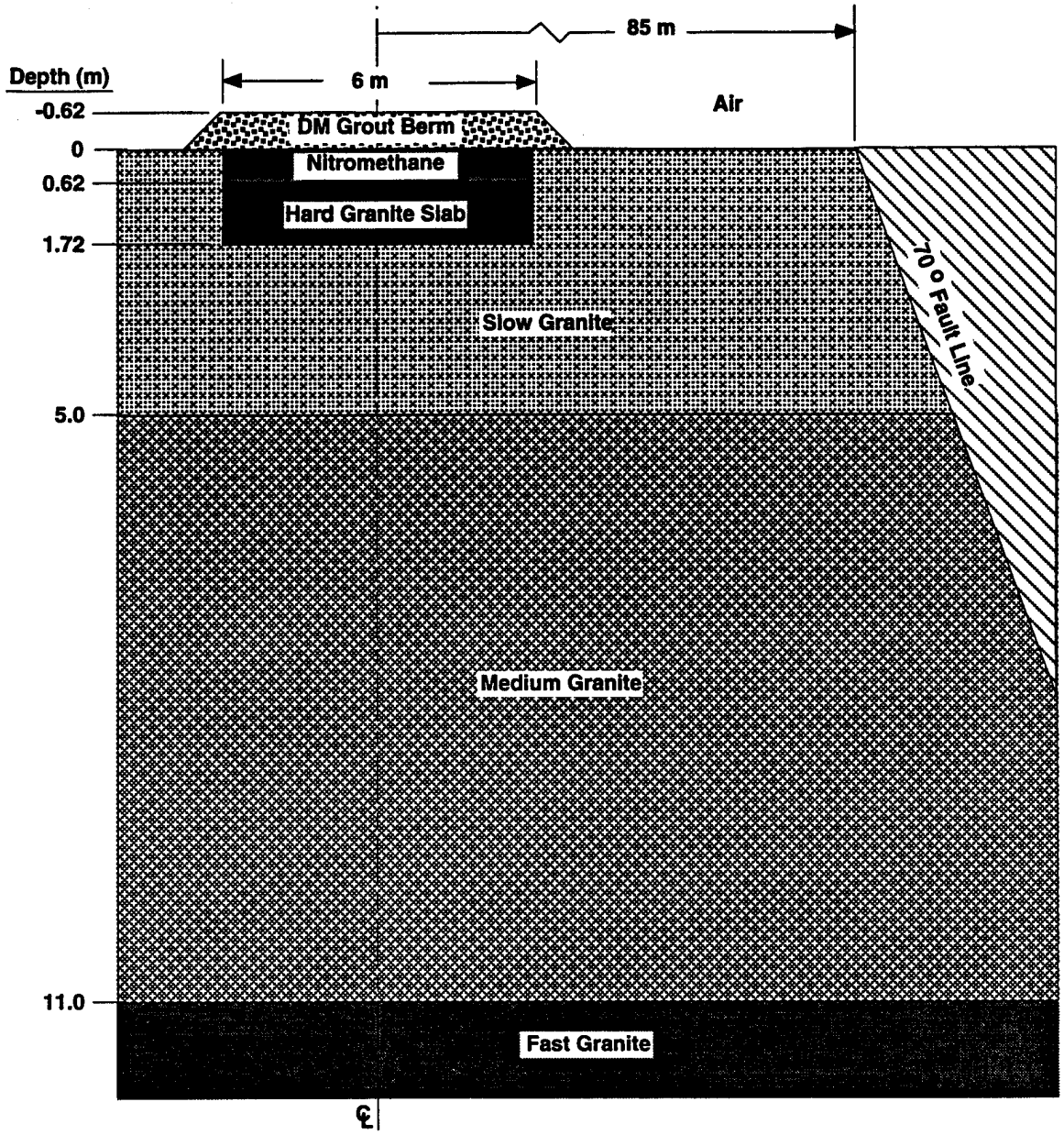

Figure 2-2. SHIST/DM4 configuration.

The test site geology for the SHIST/DM4 calculation was the same as that used in the SHIST calculation. As in the SHIST calclualtion, the fault line was not included in the 2-D calculation.

2.3 EQUATION-OF-STATE MODELS.

A Mie-Gruneisen equation-of-state (EOS) model along with a pressure-dependent yield surface was used to model the material-response behavior of the granites, crushed-rock backfill and grout materials. To describe the crush-up of the air-filled porosity in these materials, the P-α model (Hermann, 1968) was used to modify the P-V behavior of the Mie-Gruneisen model at low pressures.

The Mie-Gruneisen model used here had the following form:

$$P(\rho, E) = A\mu + B\mu^2 + \Gamma\rho E \ ,$$

where the variables are

P = pressure,
ρ = density,
E = specific energy,
$\mu = \frac{\rho}{\rho_0} - 1$,

and the input parameters are

ρ_0 = initial density,
A and B = bulk modulus coefficients,
Γ = Gruneisen constant.

The pressure dependent yield surface with the following form was used for the strength model:

$$Y(P) = Y_0 + Y_m \bullet \min(P_{max}, P) \ ,$$

where Y_0, Y_m, and P_{max} are input parameters.

The Mie-Gruneisen model coefficients, the yield surface parameters, the air-filled porosity φ, the zero-pressure sound speed c_0, and the Poisson's ratio* for the materials used in these calculations are provided in Table 2-2. The Mie-Gruneisen parameters for all of the

* A constant Poisson's ratio was used in these calculations.

granites and the crushed-rock backfill are the same; the parameters of the P-α model used to describe the crush-up of the air-filled voids were adjusted to give the zero-pressure sound speed listed in the table.

A simple tensile failure model was also used for these materials. For the granites and the grout, tensile failure occurred at a tension of 100 bars. The backfill failed immediately upon going into tension.

Table 2-2. Material property model coefficients.

Material	ρ_0 (g/cc)	A (kbar)	B (kbar)	Γ	φ	c_0 (km/s)	ν	Y_0 (kbar)	Y_m	P_{max} (kbar)
Slow Granite	2.62	500	0	0.75	0.01	1.6	0.25	0.173	0.52	5.77
Med. Granite	2.62	500	0	0.75	0.01	2.2	0.25	0.173	0.52	5.77
Fast Granite	2.62	500	0	0.75	0.01	3.4	0.25	0.173	0.52	5.77
Grout	2.41	93.3	651	0.75	0	2.3	0.37	0.136	0.17	3.0
Backfill	2.12	500	0	0.75	0.2	1.2	0.25	0.173	0.52	5.77
DM4 Granite	2.65	500	0	0.75	0	5.8	0.25	0.173	0.52	5.77

The JWL EOS which was used to model the explosive products in both calculations has the following form:

$$P = A\left(1-\frac{\omega}{R_1 V}\right)e^{-R_1 V} + B\left(1-\frac{\omega}{R_2 V}\right)e^{-R_2 V} + \frac{\omega E}{V},$$

where $V = \rho_0 / \rho$ is the relative volume, and A, B, R_1, R_2, and ω are input parameters. The parameters used for the QM-100R explosive used in the SHIST calculation (Rinehart, 1993) and the nitromethane used in the SHIST/DM4 calculation (Dobratz and Crawford, 1985) are provided in Table 2-3 along with the initial density ρ_0, energy density E_0, Chapman-Jouget pressure P_{CJ}, and the detonation velocity D.

Table 2-3. JWL EOS model coefficients.

Material	A (Mbar)	B (Mbar)	R_1	R_2	ω	ρ_0 (g/cm^3)	P_{CJ} (Mbar)	D (cm/μs)	E_0 (Mbar)
QM-100R	11.025	0.7450	6.5	2.835	0.56	1.509	0.200	7.42	0.065
Nitromethane	2.092	0.05689	4.4	1.2	0.3	1.128	0.125	6.28	0.051

The air above the ground surface was modeled as a gamma law gas with a constant value of $\gamma = 1.4$.

2.4 COMPUTATIONAL PROCEDURE.

For the SHIST calculation, a 1-D spherical geometry was used to model the explosive burn. Once the explosive had completely burned, the results were overlayed into the 2-D geometry. The calculation was run until the shock front reached the fault line. By that point in the calculation, the peak stresses were below the level of interest, so the calculation was terminated. If further investigation warrants, the calculation could be continued by overlaying the solution at this time into a 3-D RAGE grid with the material to right of the fault line included.

It was necessary to perform the entire SHIST/DM4 calculation in 2-D geometry since a 2-D detonation calculation was required to account for edge effects. This calculation was run until the peak stress dropped to the final peak stress level in the SHIST calculation.

SECTION 3
RESULTS

3.1 PEAK STRESS, VELOCITY AND TOA.

Color contour plots of the peak normal stress (pressure), peak particle velocity, and peak-stress time-of-arrival (TOA) are provided in Figures 3-1 through 3-12. Figures 3-1, 3-2, and 3-3 show the near-source region for the SHIST calculation. In these figures, the initial configuration and geology is represented by the solid black lines. Figures 3-4, 3-5, and 3-6 are similar to the above figures except that they show the entire test bed. For these last three figures, contour levels were chosen to illustrate late-time features. Figures 3-7 through 3-12 are similar to the previous six figures except that they provide peak normal stress, peak velocity, and ToA contour plots for the SHIST/DM4 calculation.

The near-source contour plots for both calculations indicate that the10 kbar range is within about 6 to 8 meters from the source. Thus, HYDROPLUS gauges could reliably be used within this region. For the SHIST configuration, the peak normal stress can be seen to fall off to about 50 bars slightly before the shock wave reaches the fault line. The SHIST/DM4 configuration coupled considerably less energy and falls below 50 bars much nearer to the source (> 60 meters).

The contour plots also clearly illustrate the effect the different material layers have on the wave propagation. In particular the effect of placing the SHIST/DM4 source in the low wave speed granite can be seen in the peak normal stress contours of Figures 3-10 and 3-11.

Surface spallation can also be seen from the peak velocity contours (Figure 3-5) for the SHIST calculation. This is indicated by the regions of high velocity near the surface directly above the source.

Because the SHIST/DM4 source was located at the surface, it coupled substantially less energy into far-field ground motion than the SHIST source. Therefore, it is difficult to compare the two calculations without establishing a scale factor. This is difficult because the site layering introduces characteristic distances (layer thicknesses) that do no scale. However, we have attempted to obtain a crude estimate for a scale factor by comparing the peak variables along the axis directly below the source.

In Figures 3-13a, 3-14a, and 3-15a we have plotted the peak normal stress, peak velocity and peak-stress ToA along the symmetry axis below the source for both calculations. The effect of the layer interfaces at 5 amd 16 meters can be seen to some extent, but the dominant feature in these curves is the source-geometry effect seen in the SHIST/DM4 results above about 10 meters.

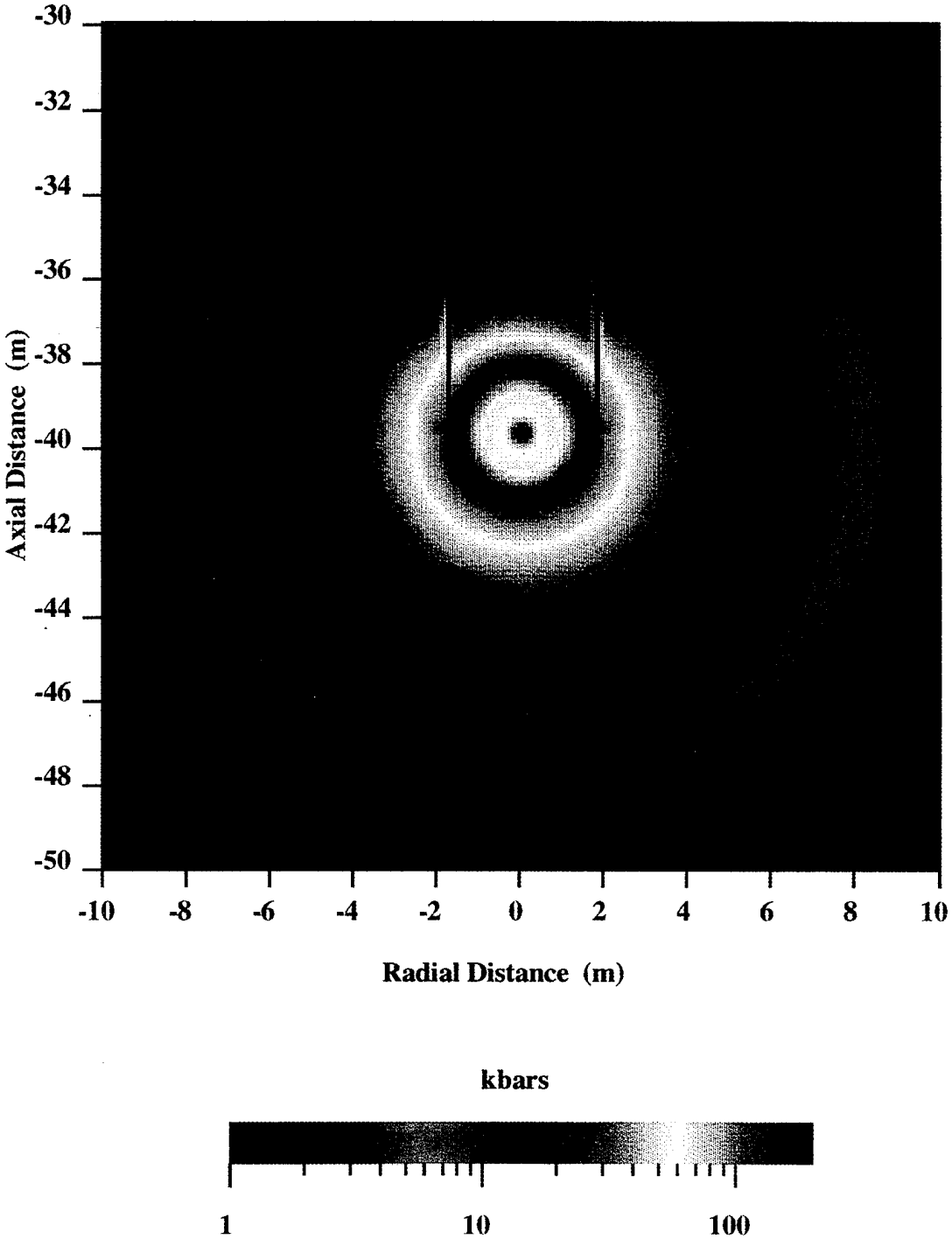

Figure 3-1. Near-field peak normal stress contours for the SHIST simulation.

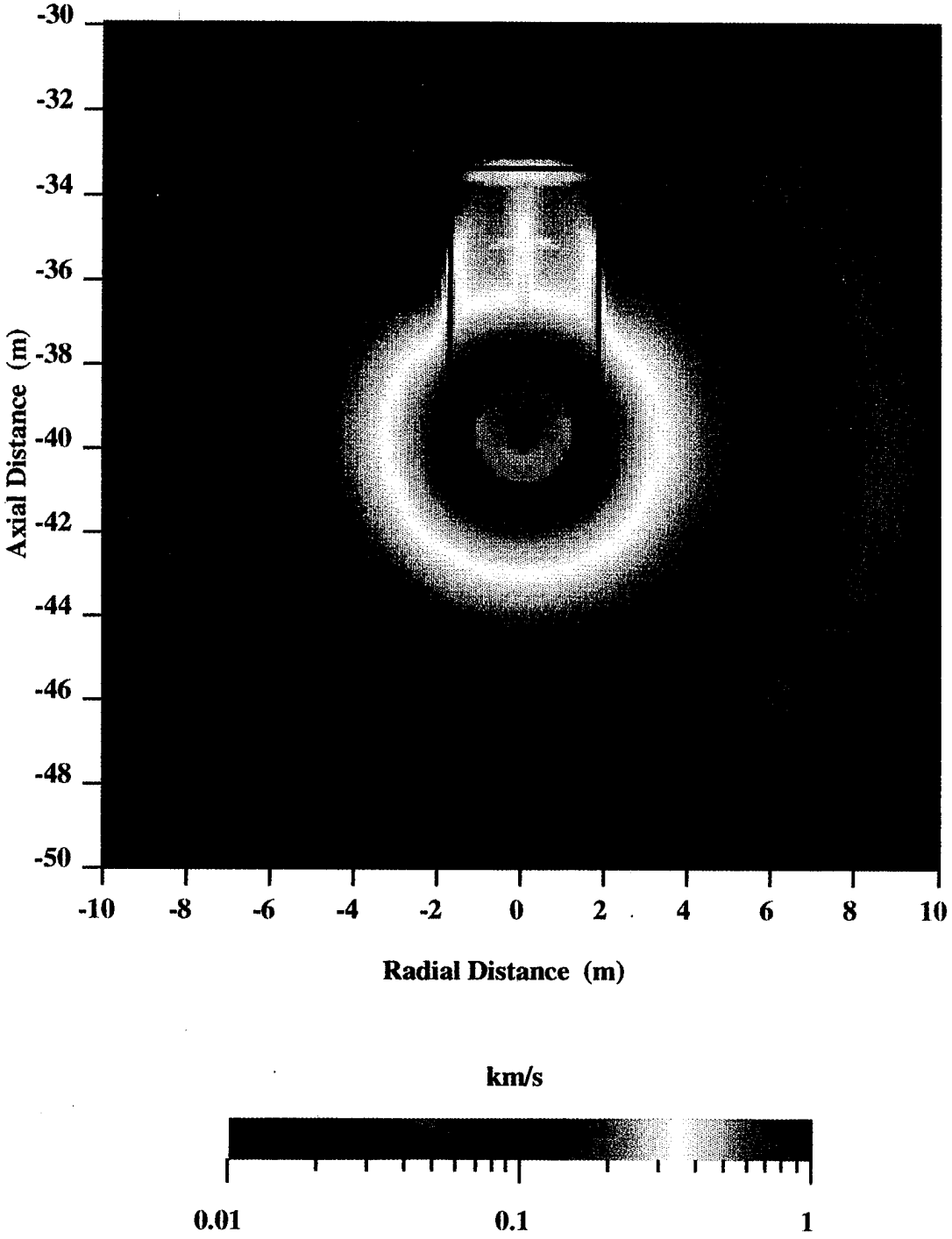

Figure 3-2. Near-field peak particle velocity contours for the SHIST simulation.

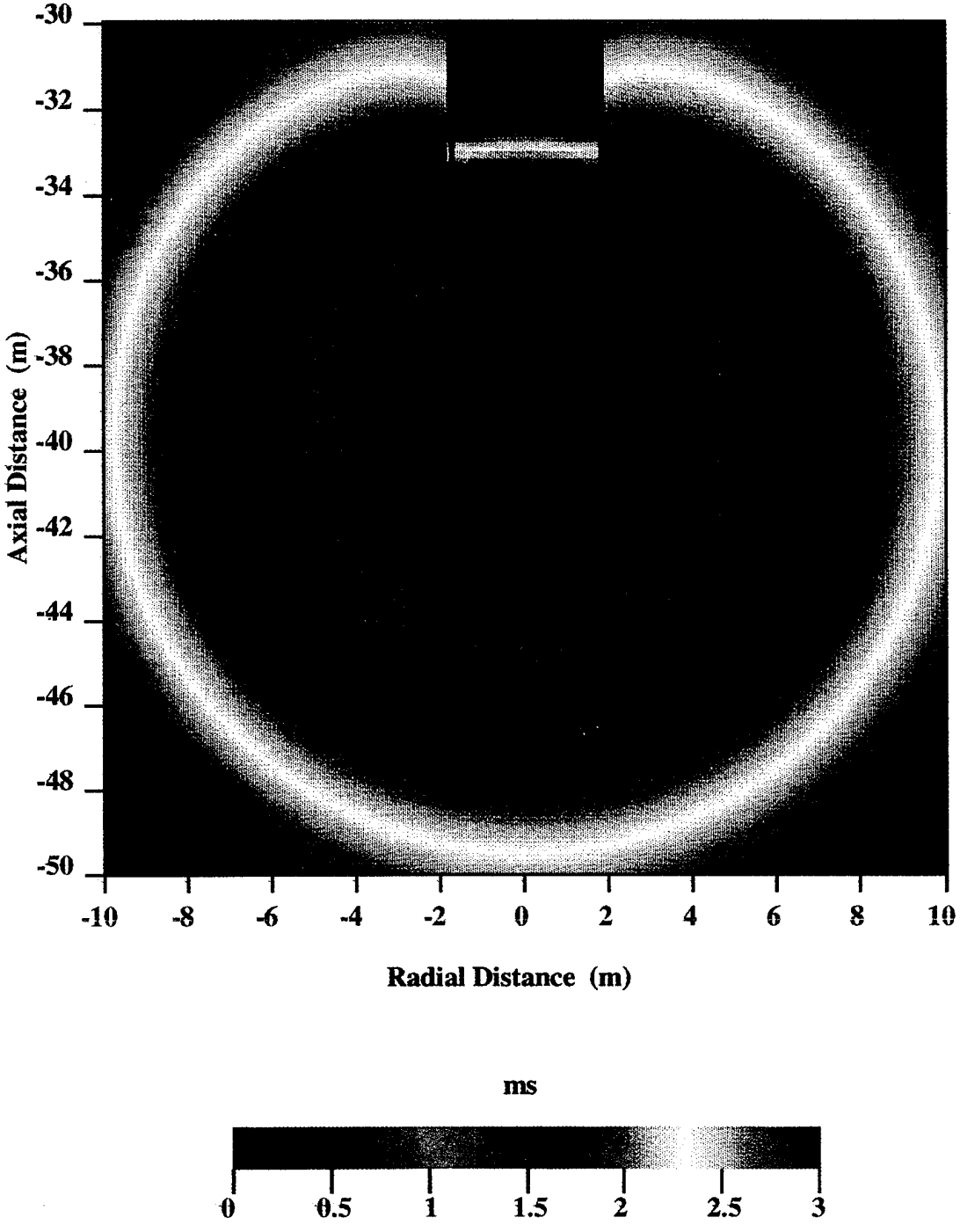

Figure 3-3. Near-field time-of-arrival contours for the SHIST simulation.

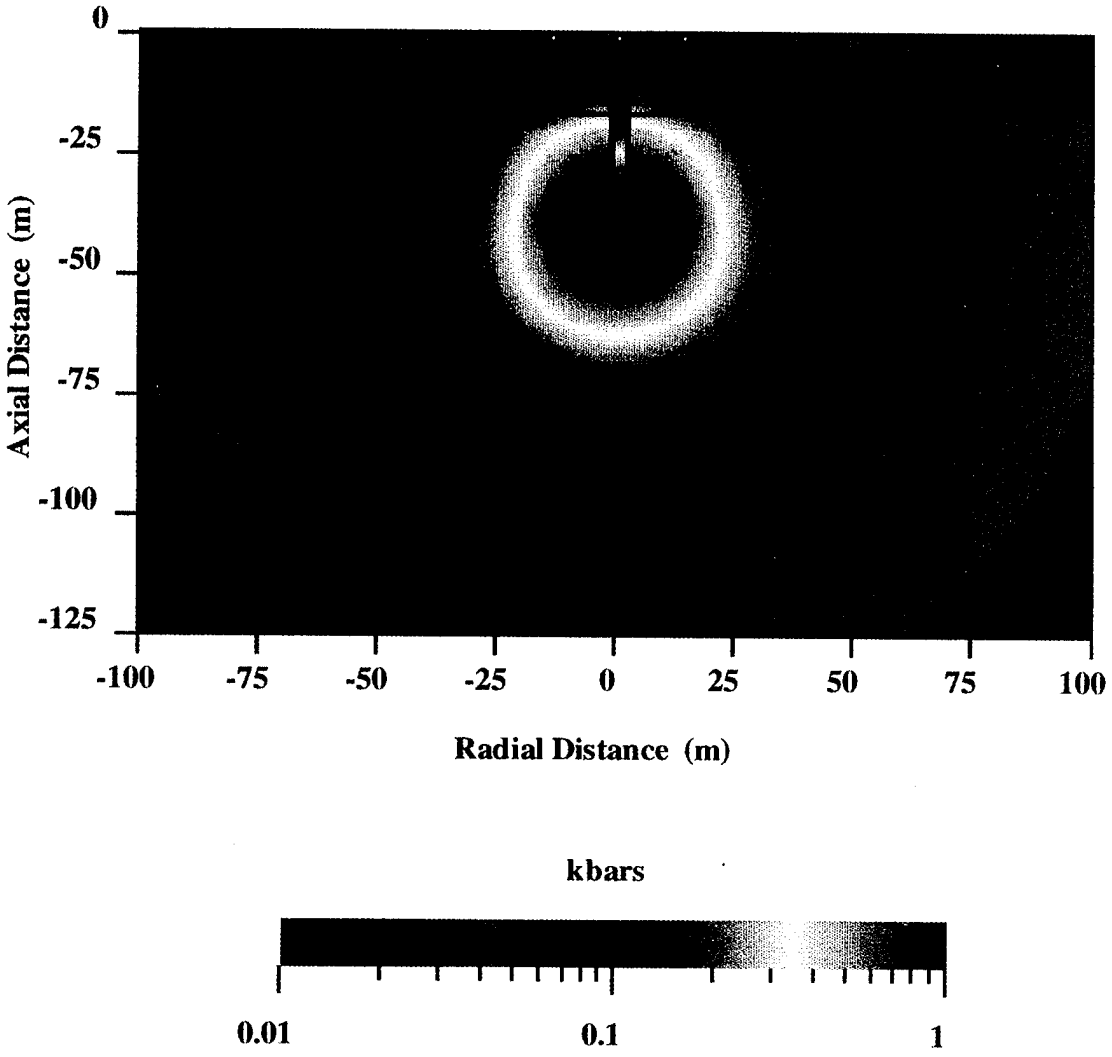

Figure 3-4. Far-field peak normal stress contours for the SHIST simulation.

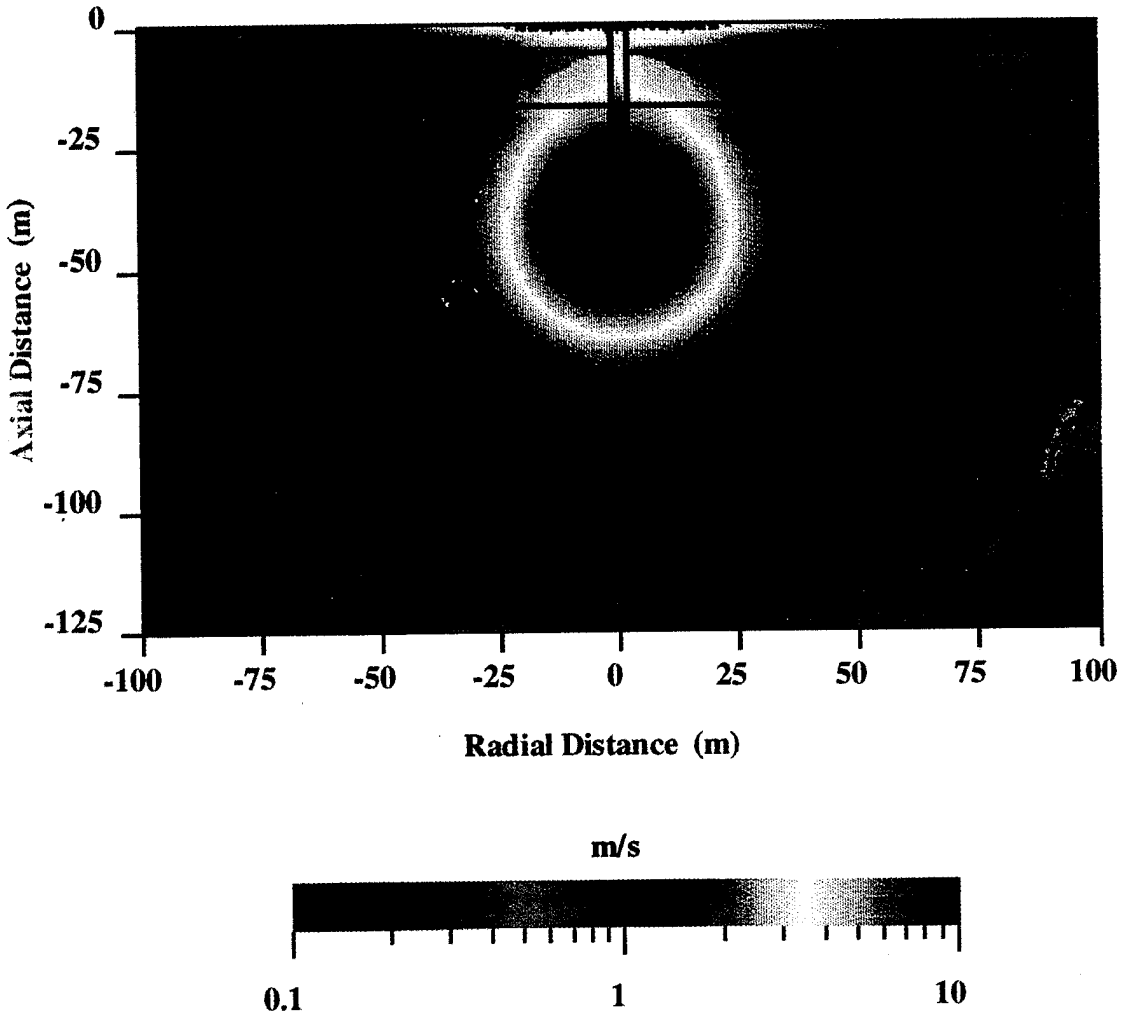

Figure 3-5. Far-field peak particle velocity contours for the SHIST simulation.

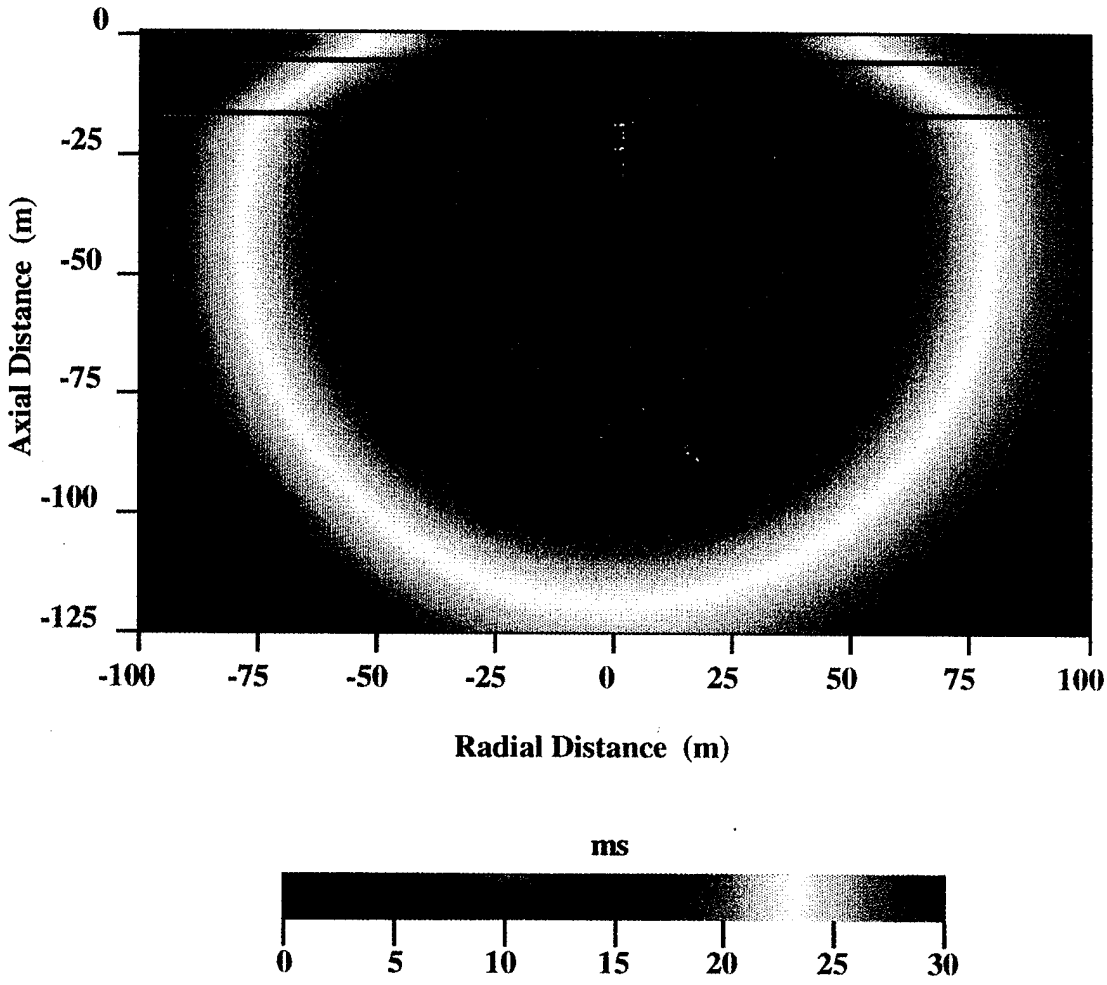

Figure 3-6. Far-field time-of-arrival contours for the SHIST simulation.

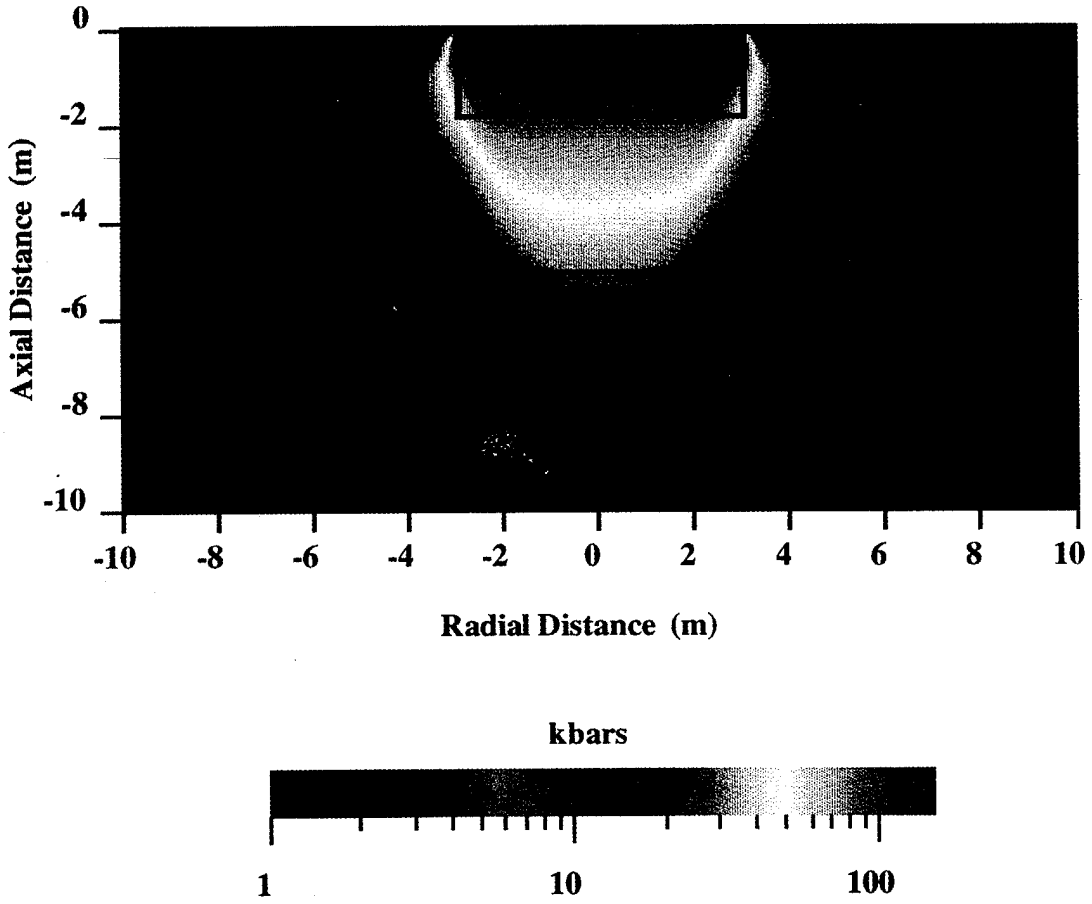

Figure 3–7. Near-field peak normal stress contours for the SHIST/DM4 simulation.

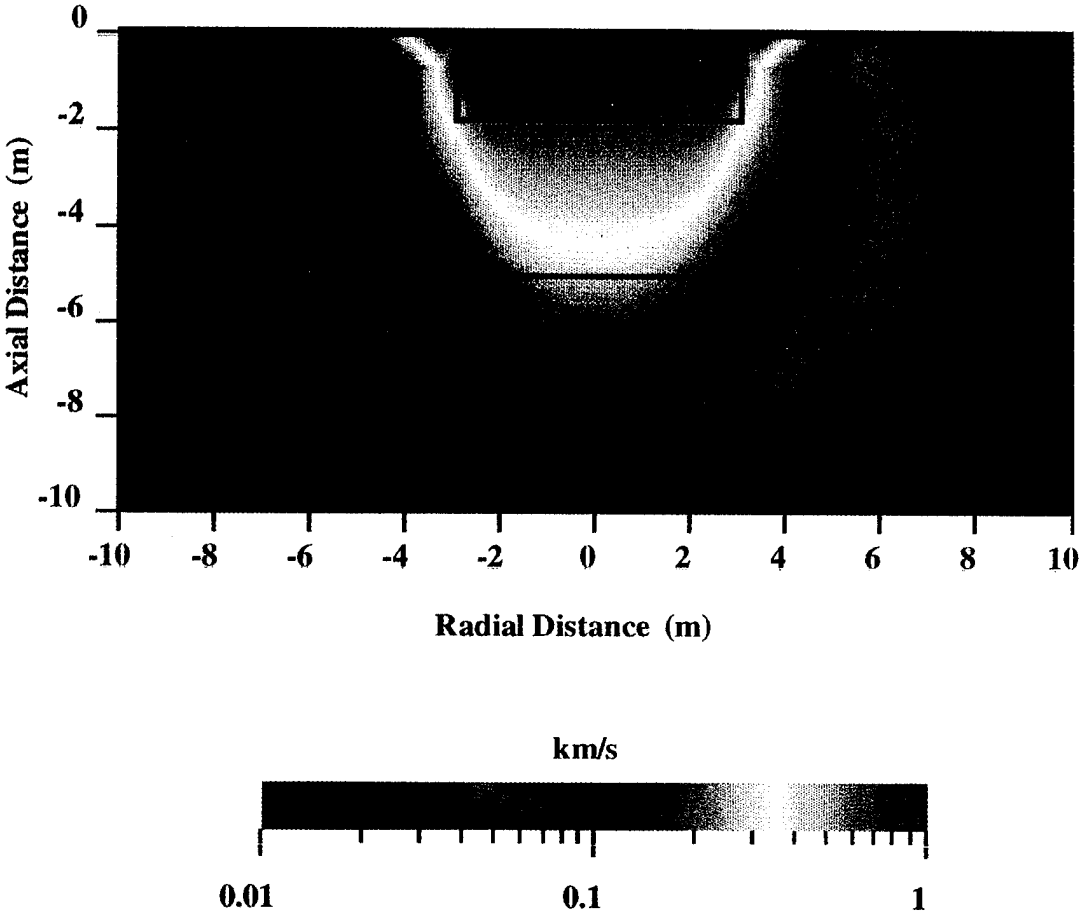

Figure 3–8 Near-field peak particle velocity contours for the SHIST/DM4 simulation.

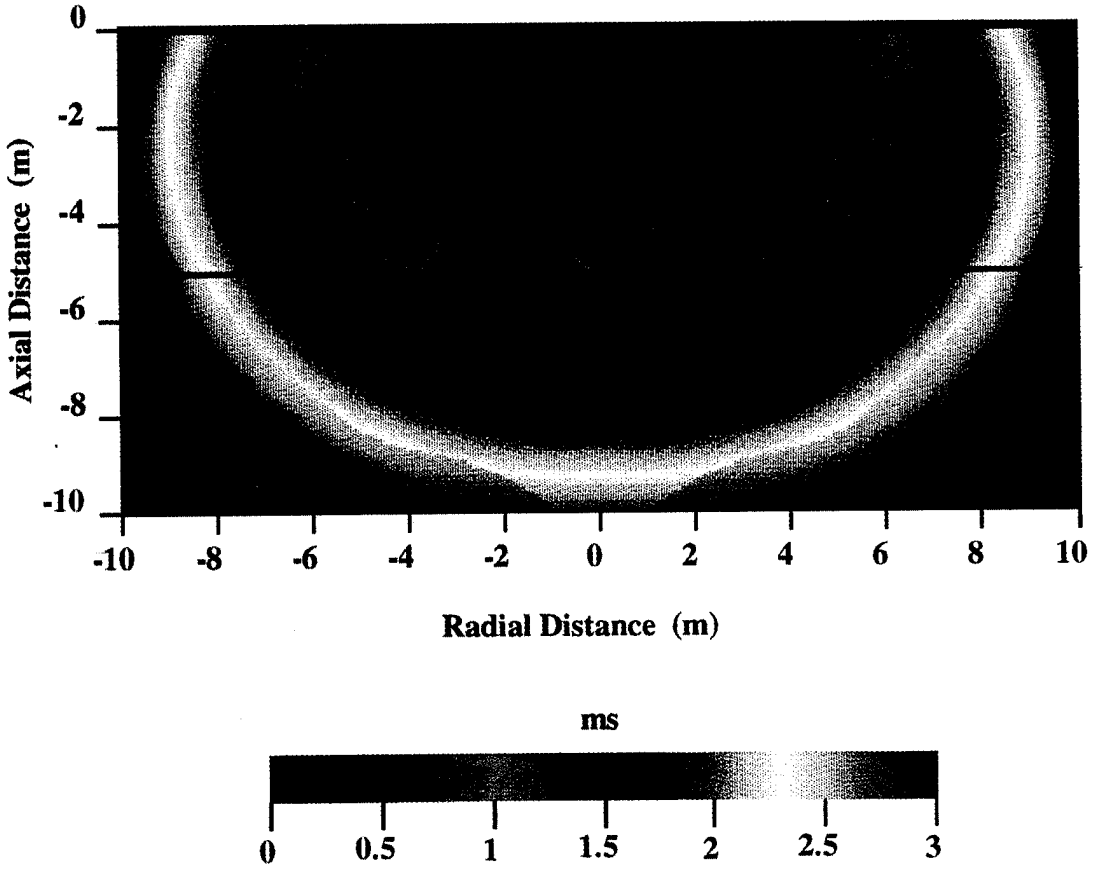

Figure 3-9. Near-field time-of-arrival contours for the SHIST/DM4 simulation.

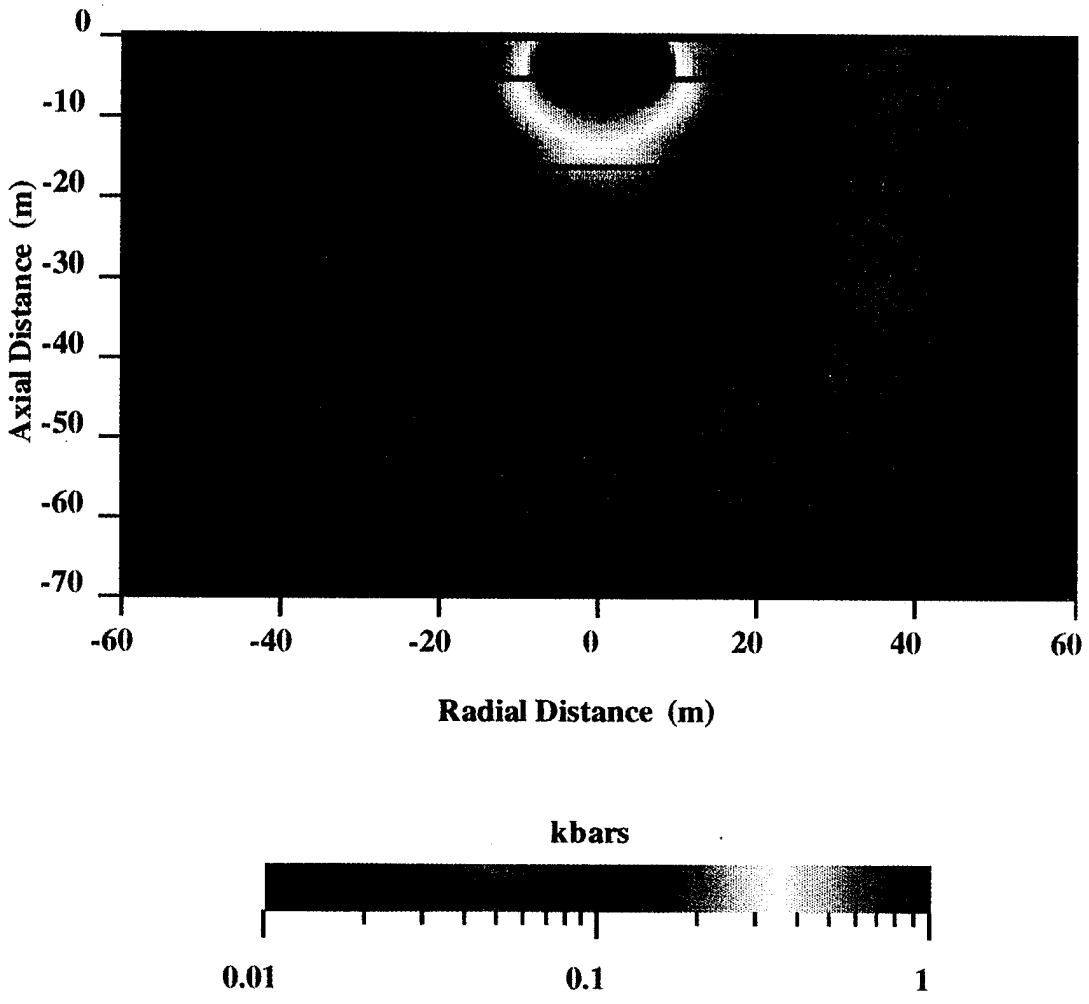

Figure 3-10. Far-field peak normal stress contours for the SHIST/DM4 simulation.

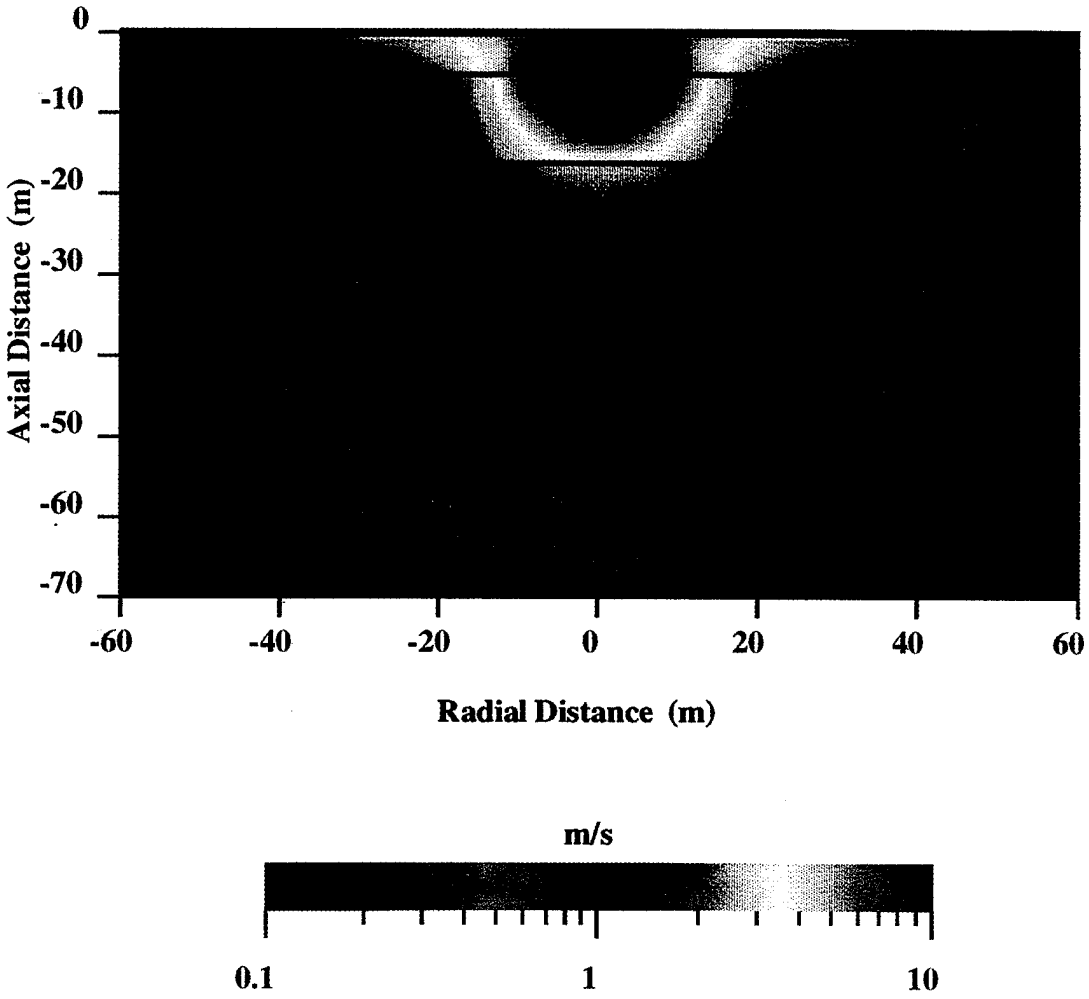

Figure 3–11. Far-field peak particle velocity contours for the SHIST/DM4 simulation.

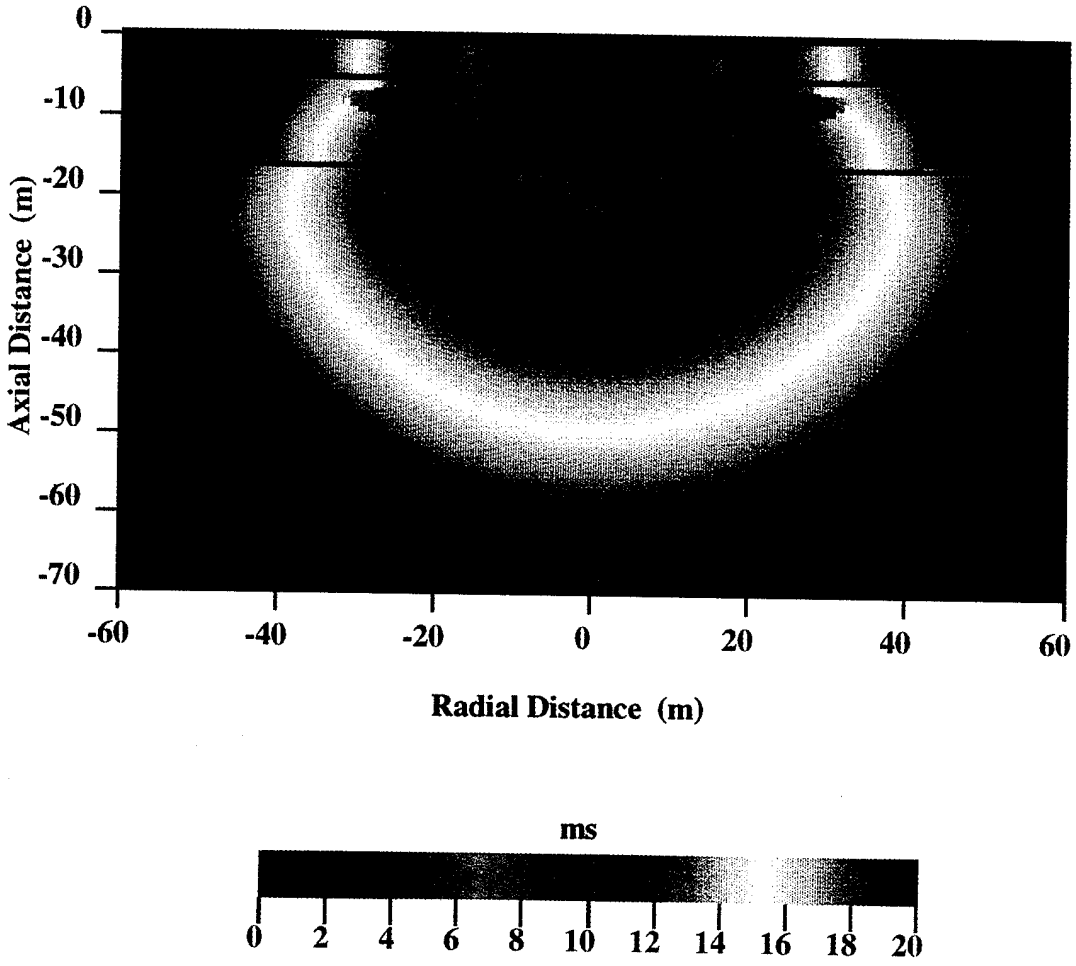

Figure 3-12. Far-field time-of-arrival contours for the SHIST/DM4 simulation.

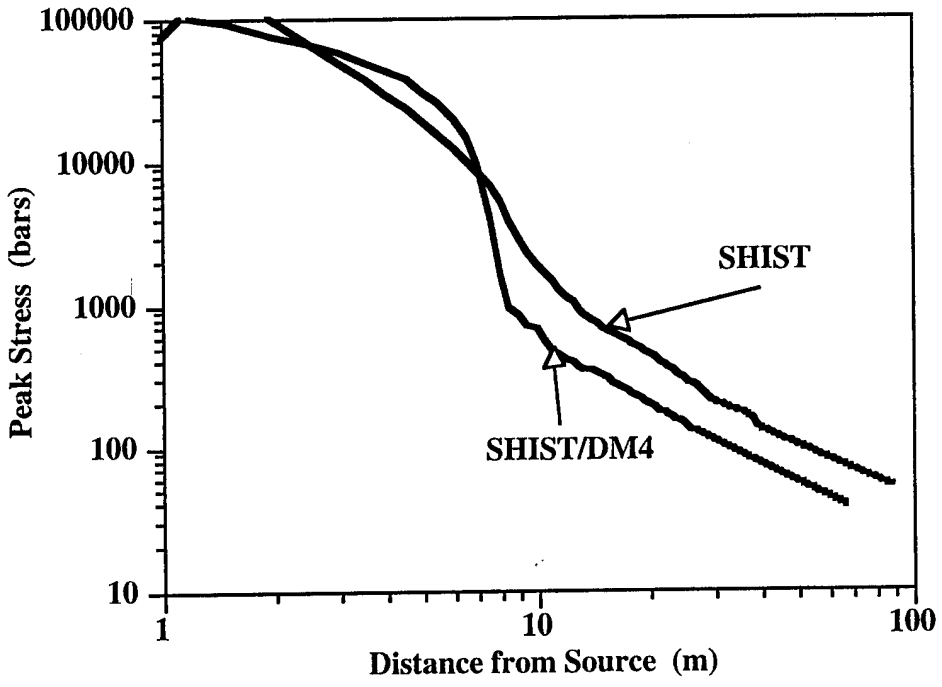

a.

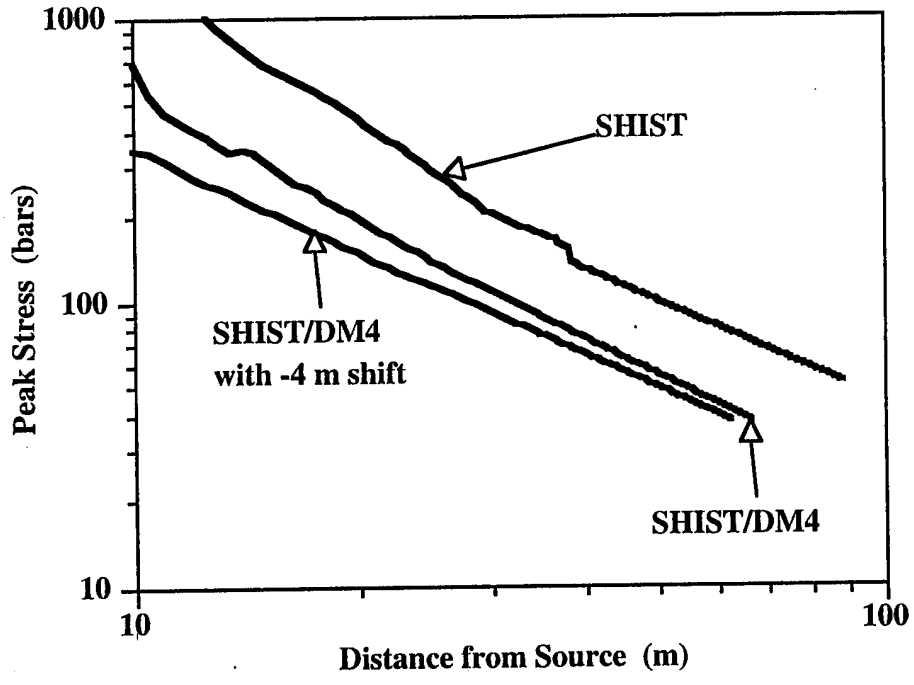

b.

Figure 3–13. Peak normal stress along the symmetry axis below the source for the SHIST and SHIST/DM4 calculations.

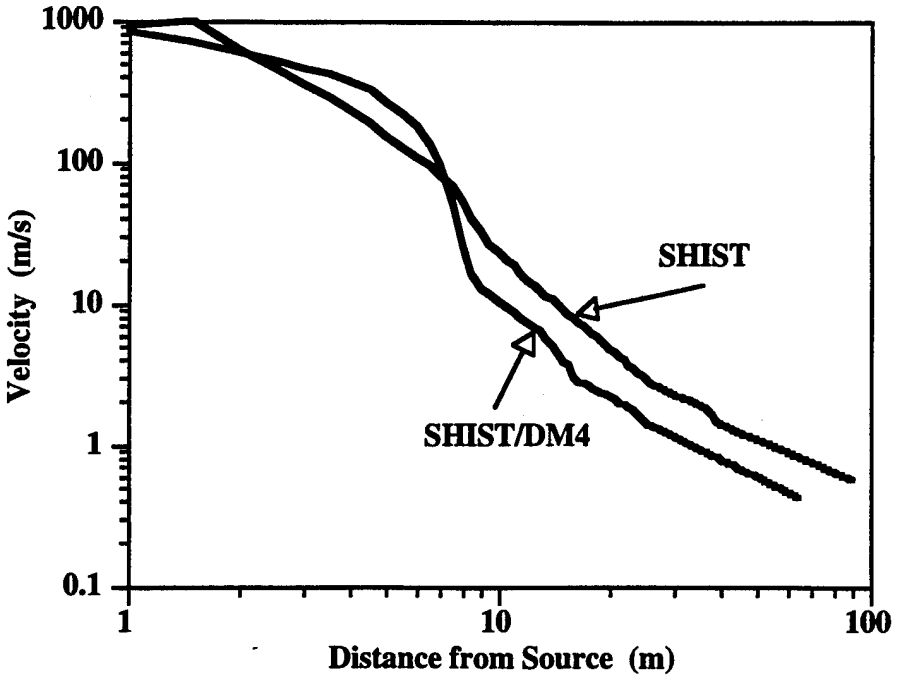

a.

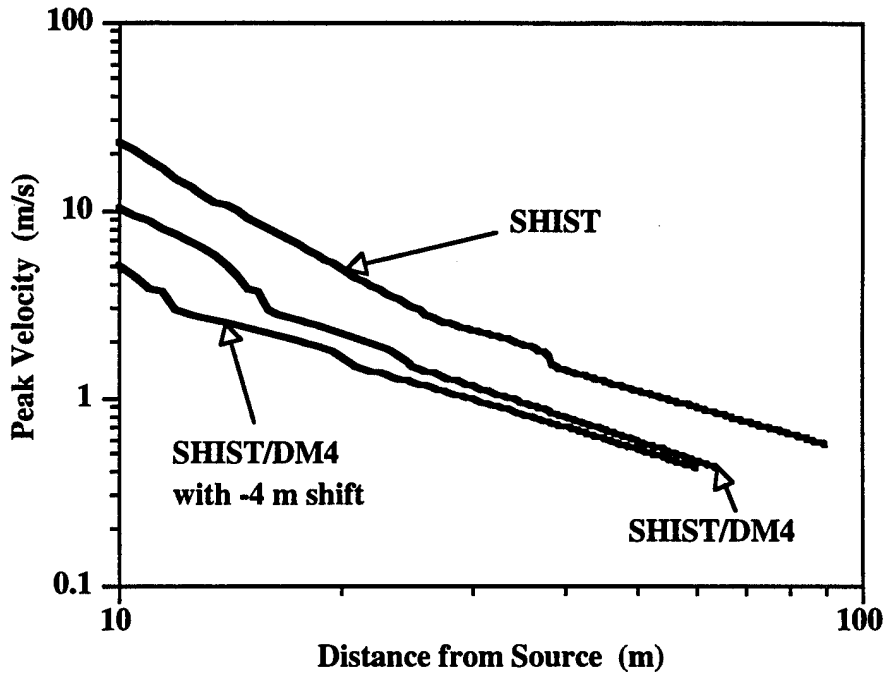

b.

Figure 3–14. Peak particle velocity along the symmetry axis below the source for the SHIST and SHIST/DM4 calculations.

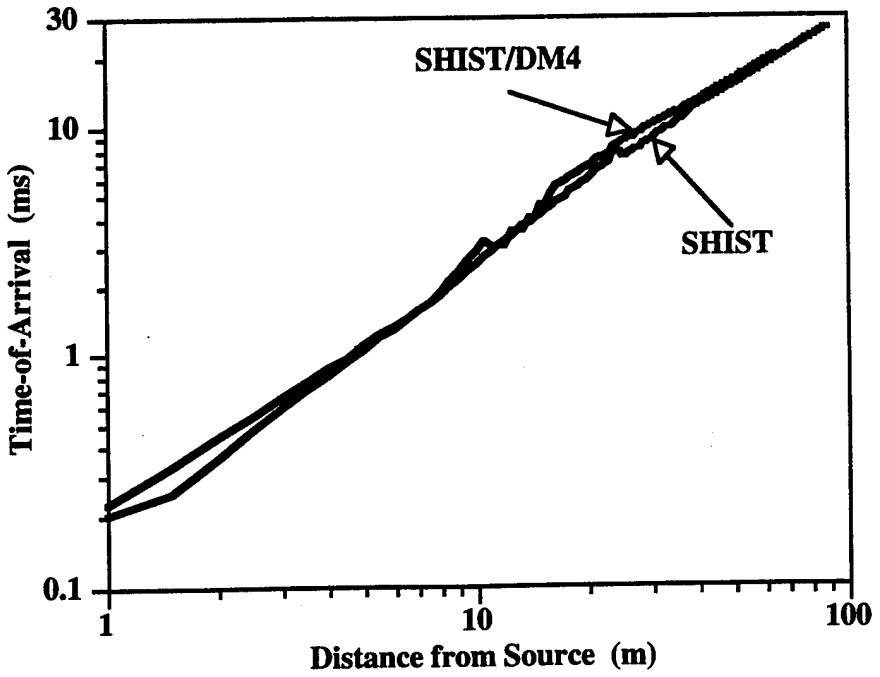

a.

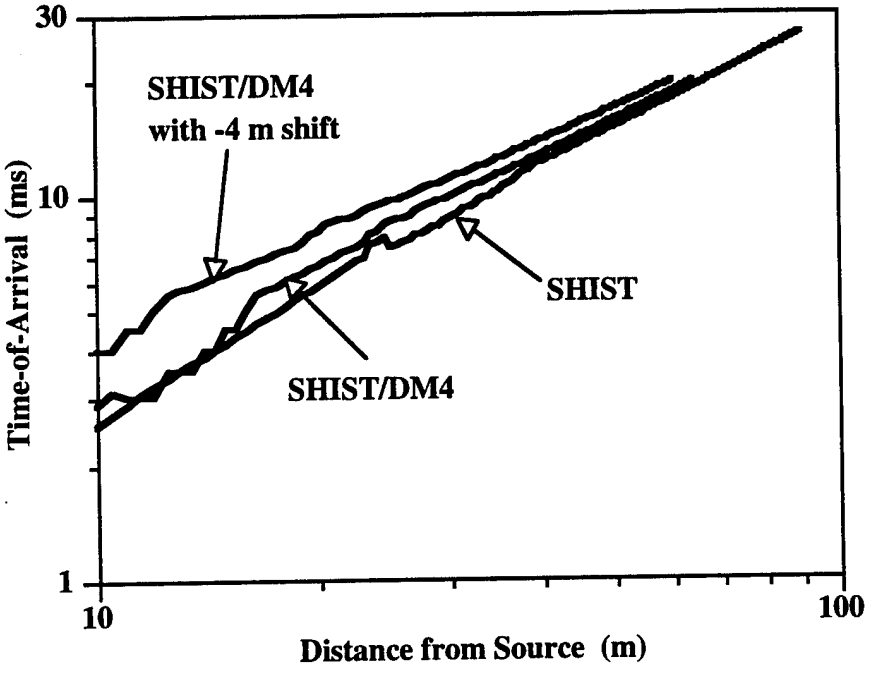

b.

Figure 3–15. Time-of-arrival along the symmetry axis below the source for the SHIST and SHIST/DM4 calculations.

Beyond about 40 meters for the SHIST calculation and 20 meters for the SHIST/DM4 calculation (i.e., below about 100 bars) the attenuation rate appears to become constant, so we attempted to derive a scale factor in this region. By assuming that the effective late-time source location for the SHIST/DM4 calculation has moved down to about 4 meters below the ground surface as a result of surface interactions, the peak stress and velocity curves for the two calculations can be made approximately parallel. This is shown in Figures 3-13b and 3-14b. Figure 3-15b shown the ToA curves with the same shift.

From the shifted peak stress and velocity curves, we can derive an energy scale factor of about 5.9 between the two calculations. That is, if the radius in SHIST/DM4 attenuation curves are cube-root scaled by a factor of $5.9^{1/3}$, then the curves for the two calculations coincide in the low-stress region. This is shown for the peak stress attenuation in Figure 3-16. This means that in the low-stress region directly below the explosions, the ground shock behaves as if the SHIST/DM4 calculation coupled only 17% as much energy as the SHIST calculation. However, because of the layering, this conclusion may not apply to the regions near the surface. The extent to which this scale factor applies to all regions of the calculations can be evaluated by comparing the scaled peak-stress contour plot for the SHIST/DM4 calculation with the SHIST peak stress countour plot provided in Figure 3-4.

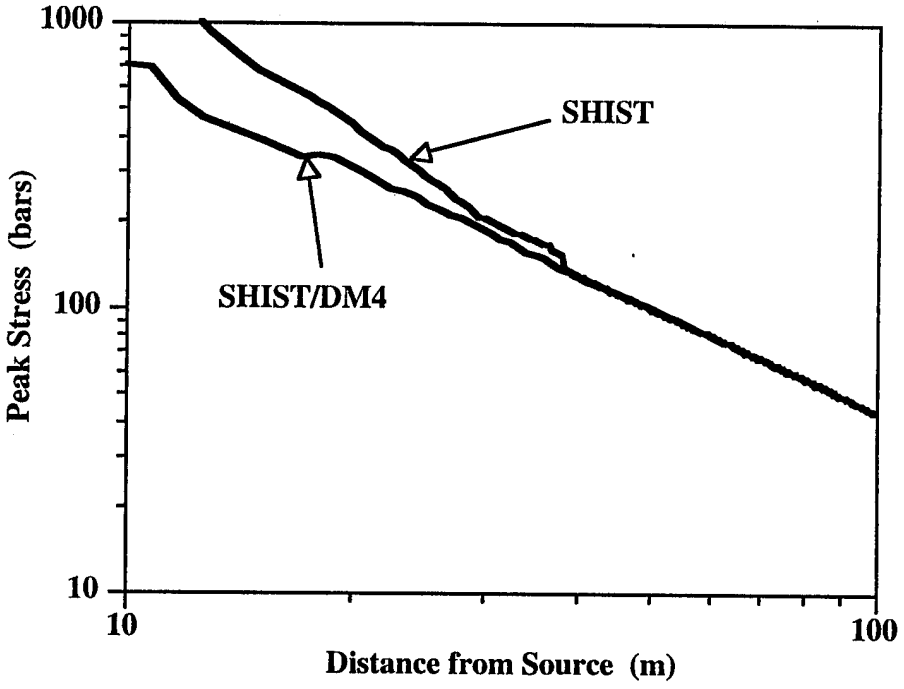

Figure 3-16. Peak normal stress along the symmetry axis below the source for the SHIST and yield scaled SHIST/DM4 calculations.

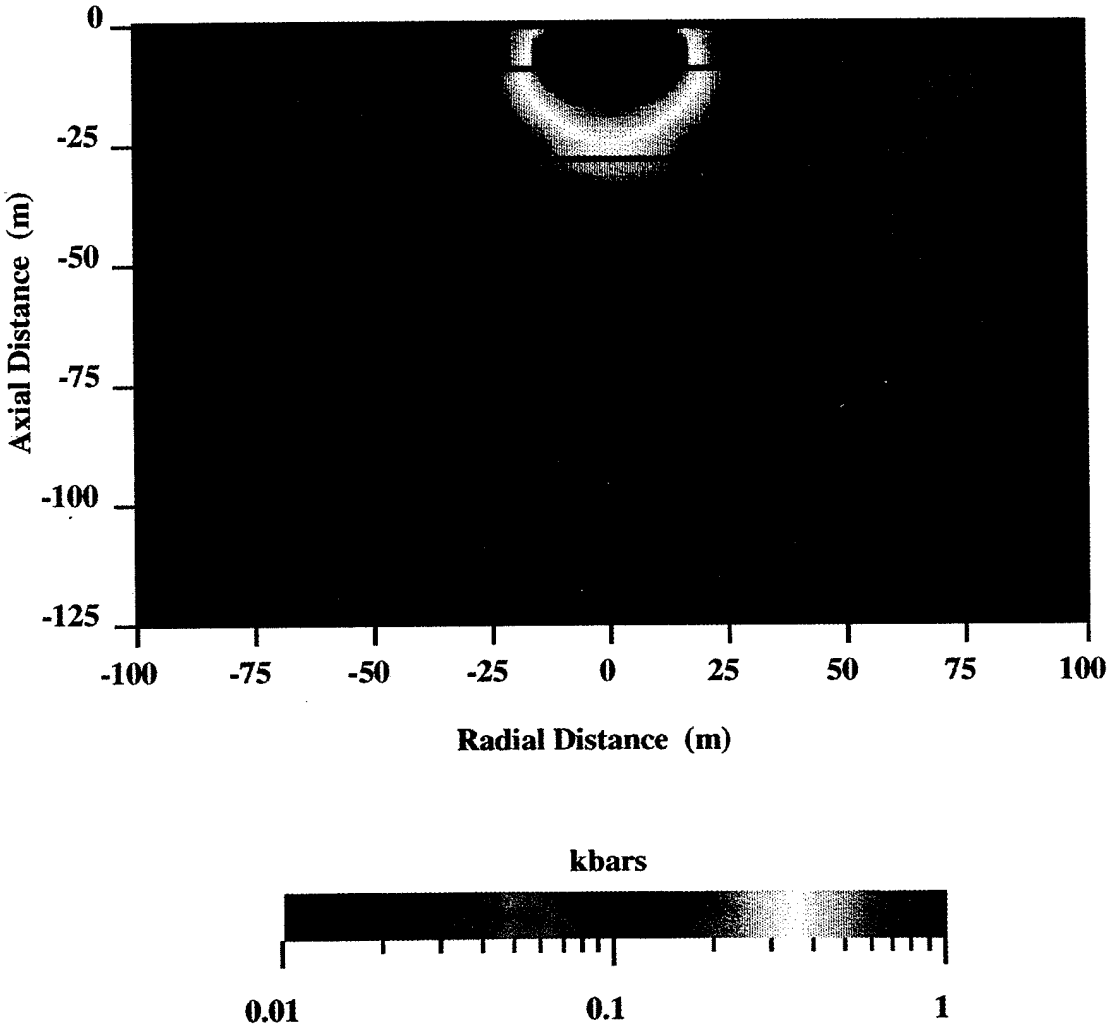

Figure 3-17. **Far-field peak normal stress contours for the SHIST/DM4 simulation scaled to the SHIST effective yield.**

3.2 TIME HISTORIES.

One of the goals of these calculations was to predict gauge response at various locations. Figure 2-1 showed the proposed gauge lines for the SHIST experiment. In Figures 3-18 through 3-38, we have provided numerous plots showing representative samples of the tracer particle stress, velocity and displacement histories. Three particle locations along each gauge line at depths of 5, 15, and 30 meters are presented. The top figure is the radial stress while the middle and bottom figures show the speed and radial particle displacement as a function of time, respectively.

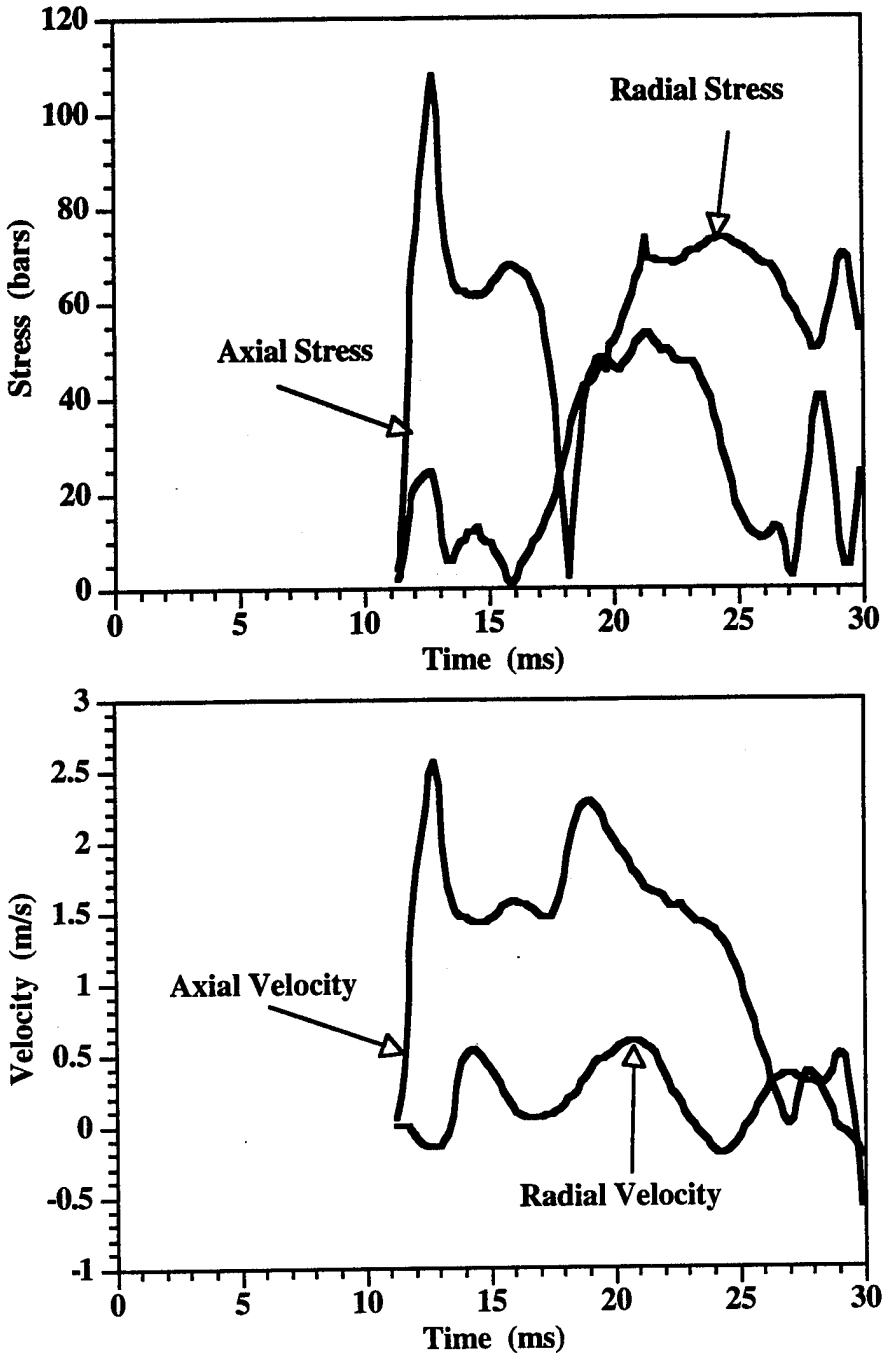

Figure 3-18. **Stress and velocity histories for the SHIST calculation at 4 meters ground range and 5 meters depth.**

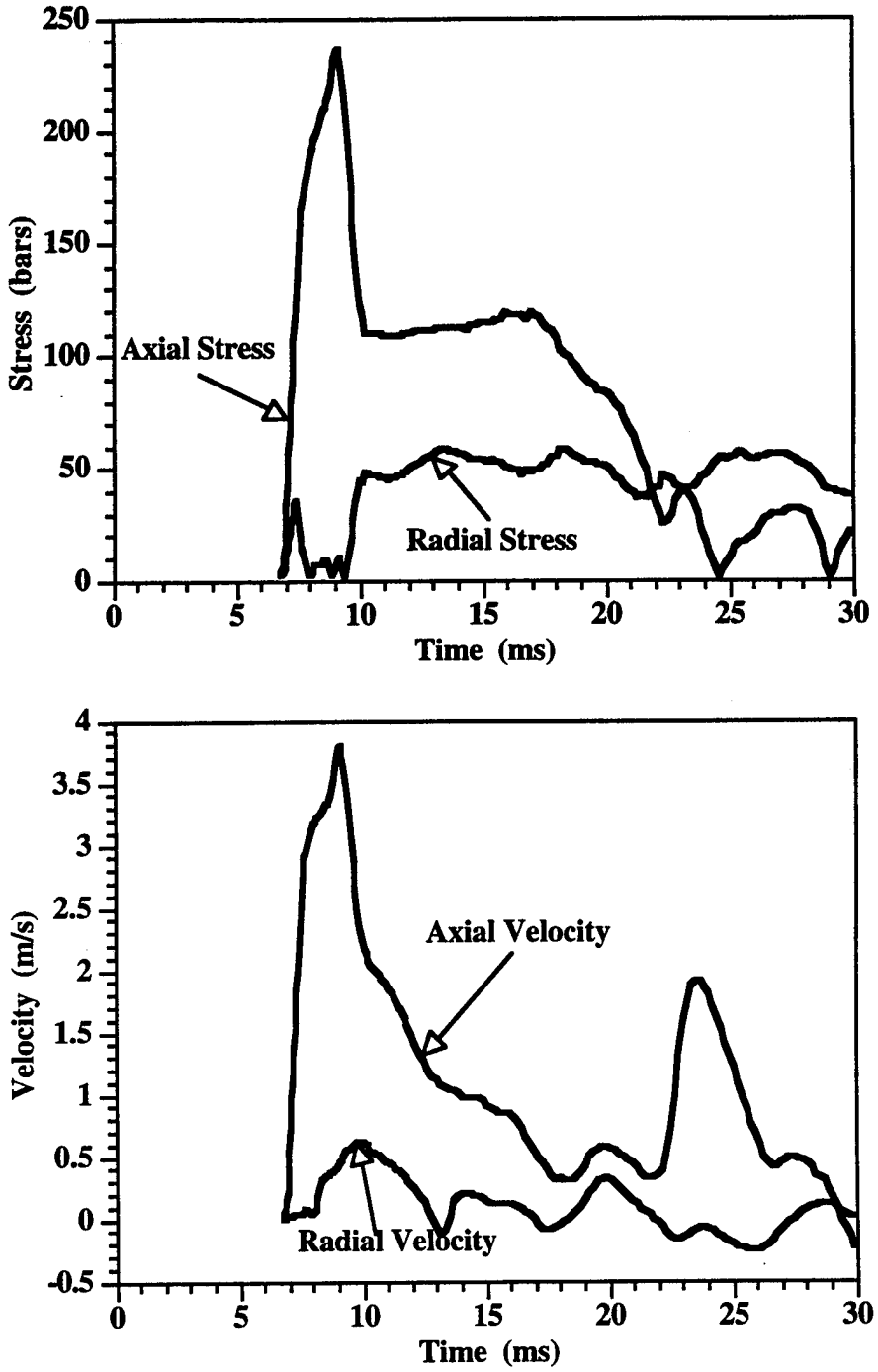

Figure 3-19. Stress and velocity histories for the SHIST calculation at 4 meters ground range and 15 meters depth.

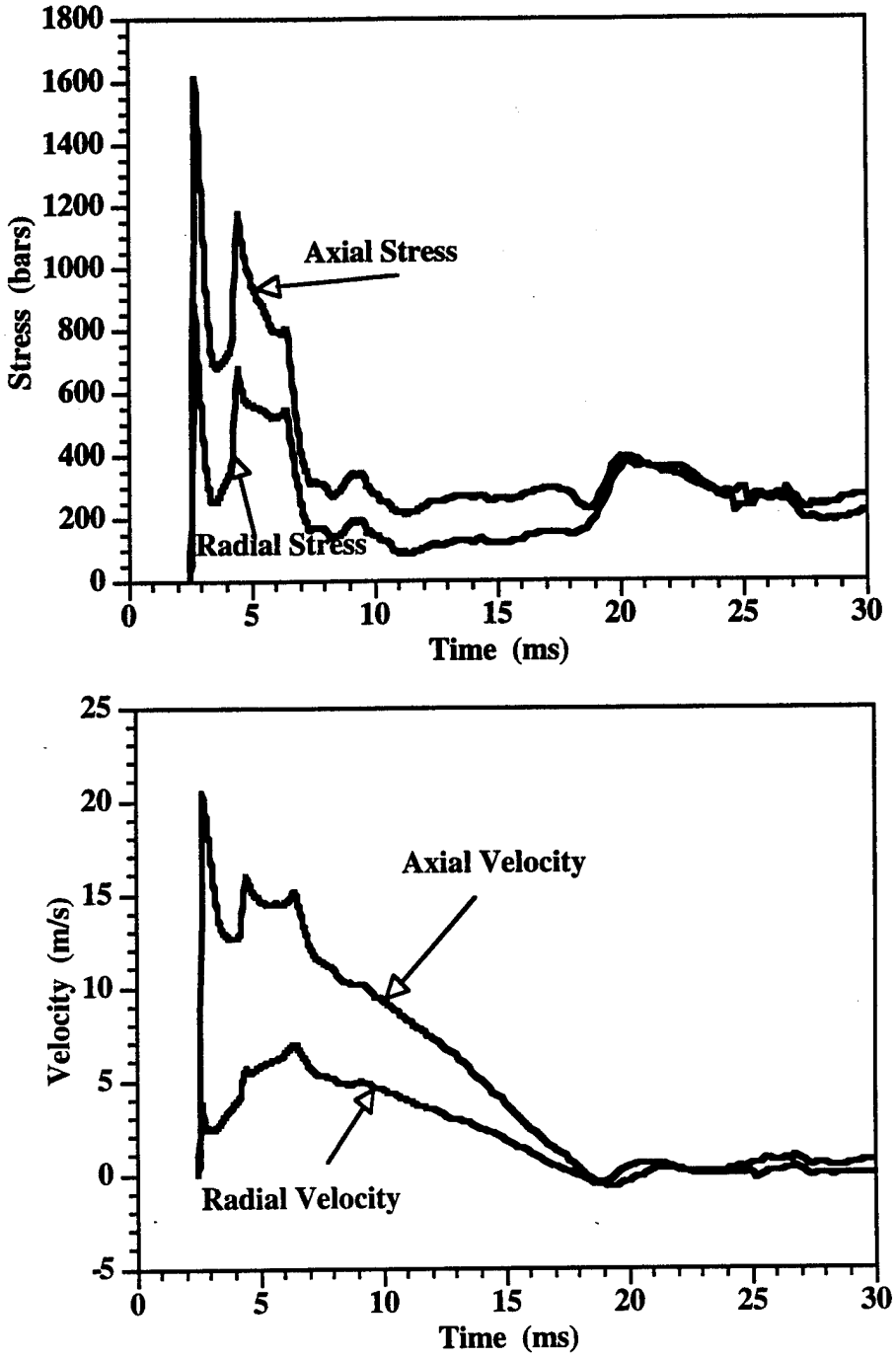

Figure 3-20. Stress and velocity histories for the SHIST calculation at 4 meters ground range and 30 meters depth.

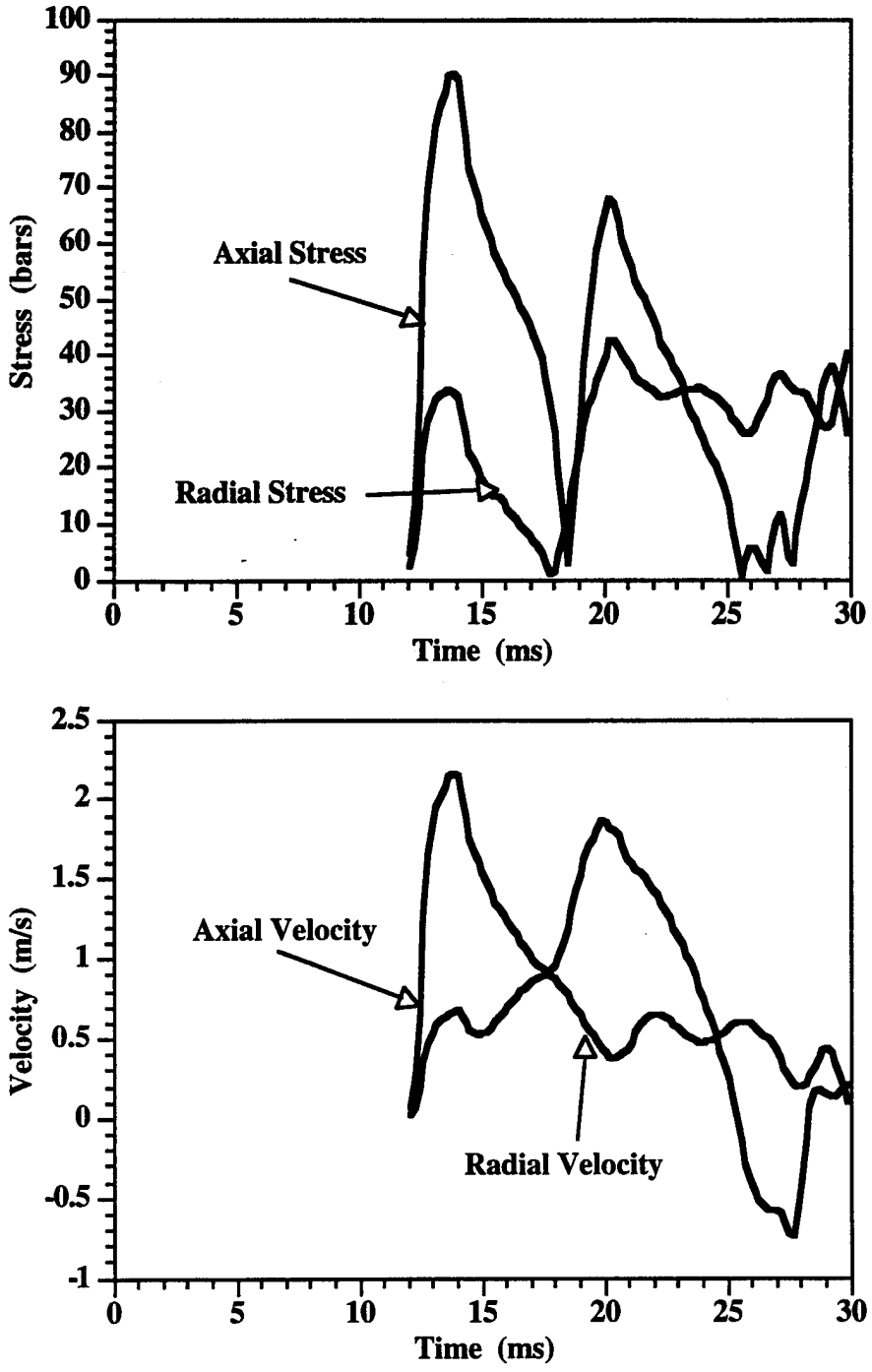

Figure 3-21. Stress and velocity histories for the SHIST calculation at 15 meters ground range and 5 meters depth.

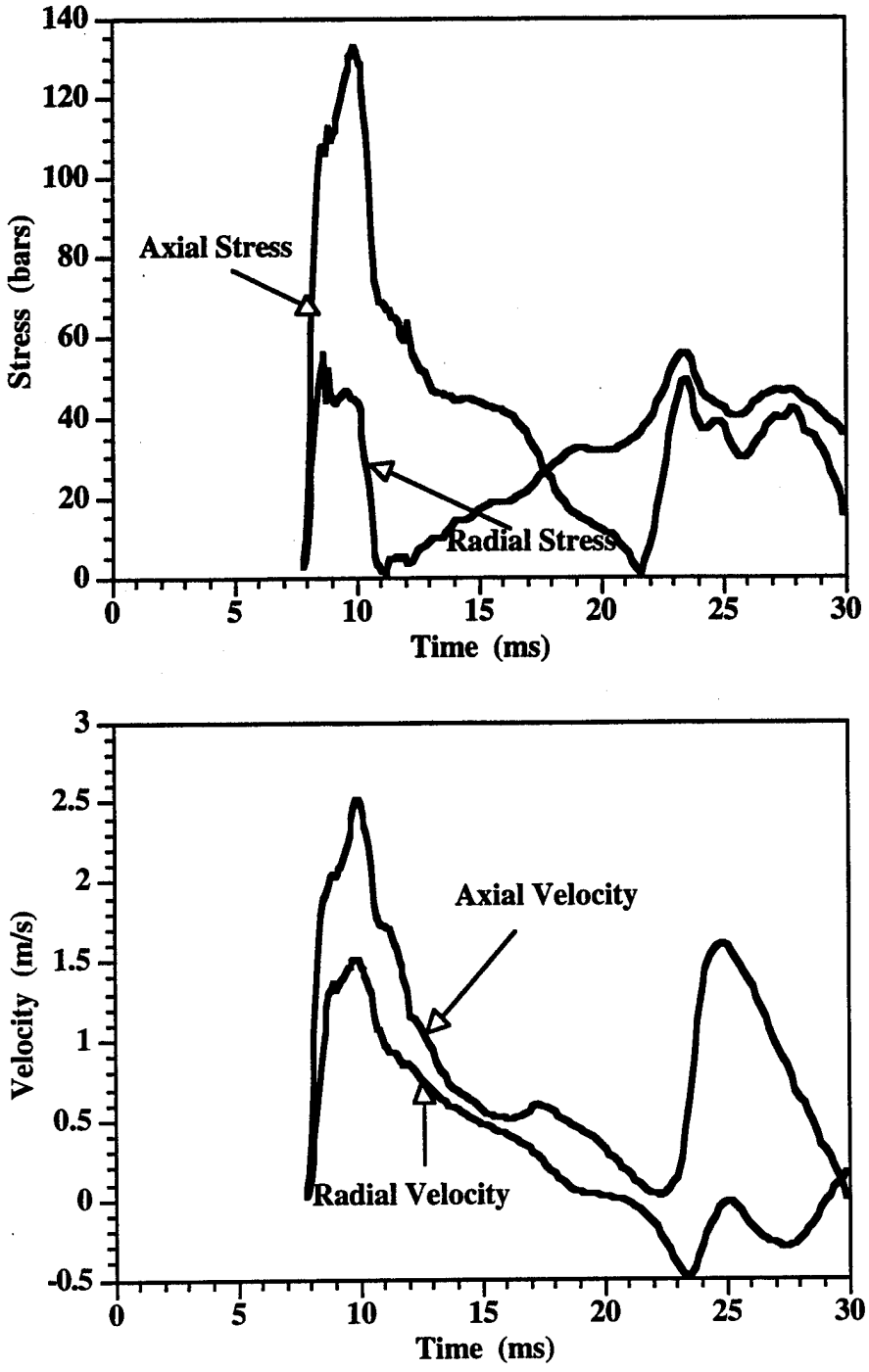

Figure 3-22. **Stress and velocity histories for the SHIST calculation at 15 meters ground range and 15 meters depth.**

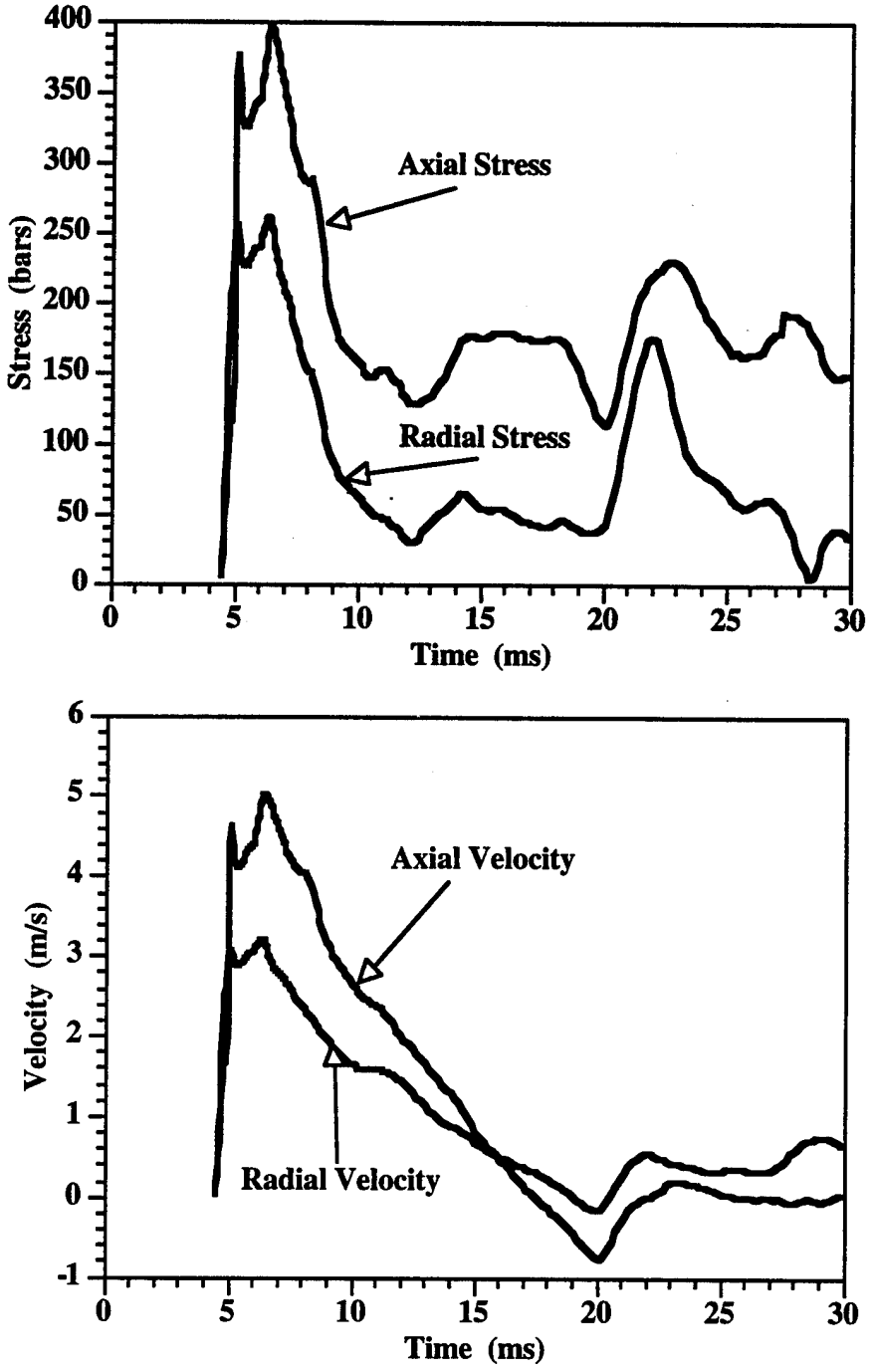

Figure 3-23. Stress and velocity histories for the SHIST calculation at 15 meters ground range and 30 meters depth.

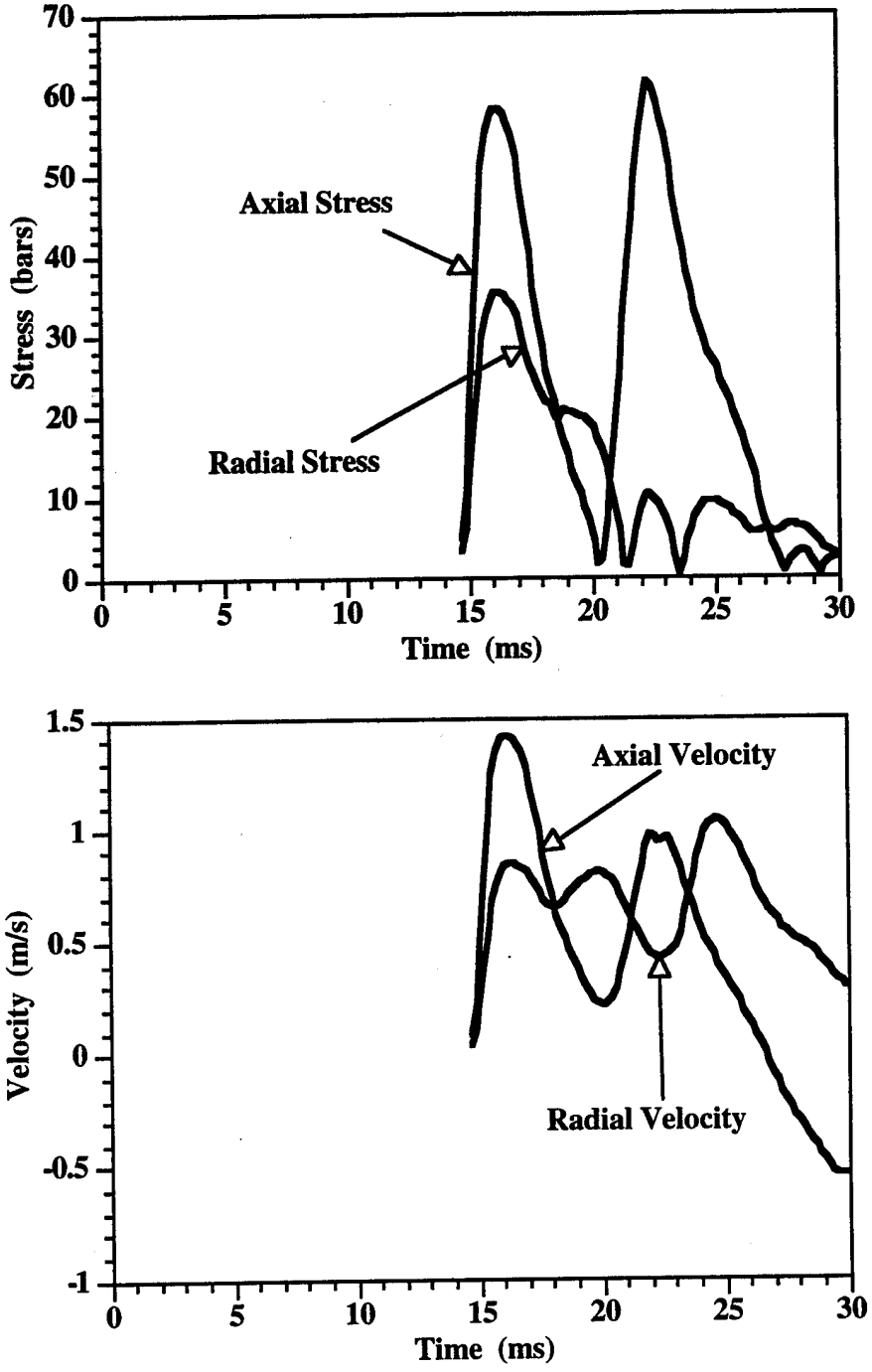

Figure 3-24. Stress and velocity histories for the SHIST calculation at 30 meters ground range and 5 meters depth.

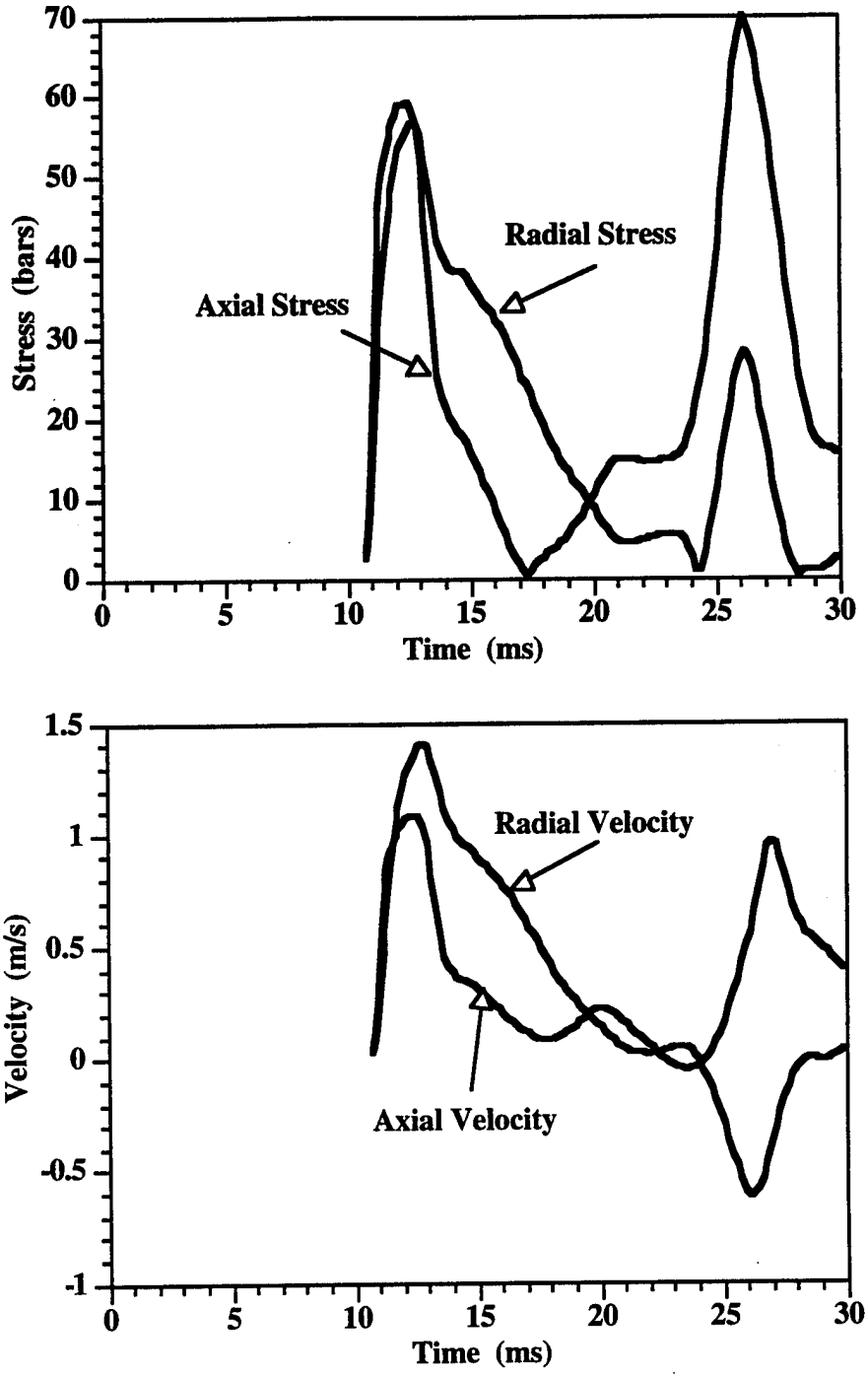

Figure 3-25. Stress and velocity histories for the SHIST calculation at 30 meters ground range and 15 meters depth.

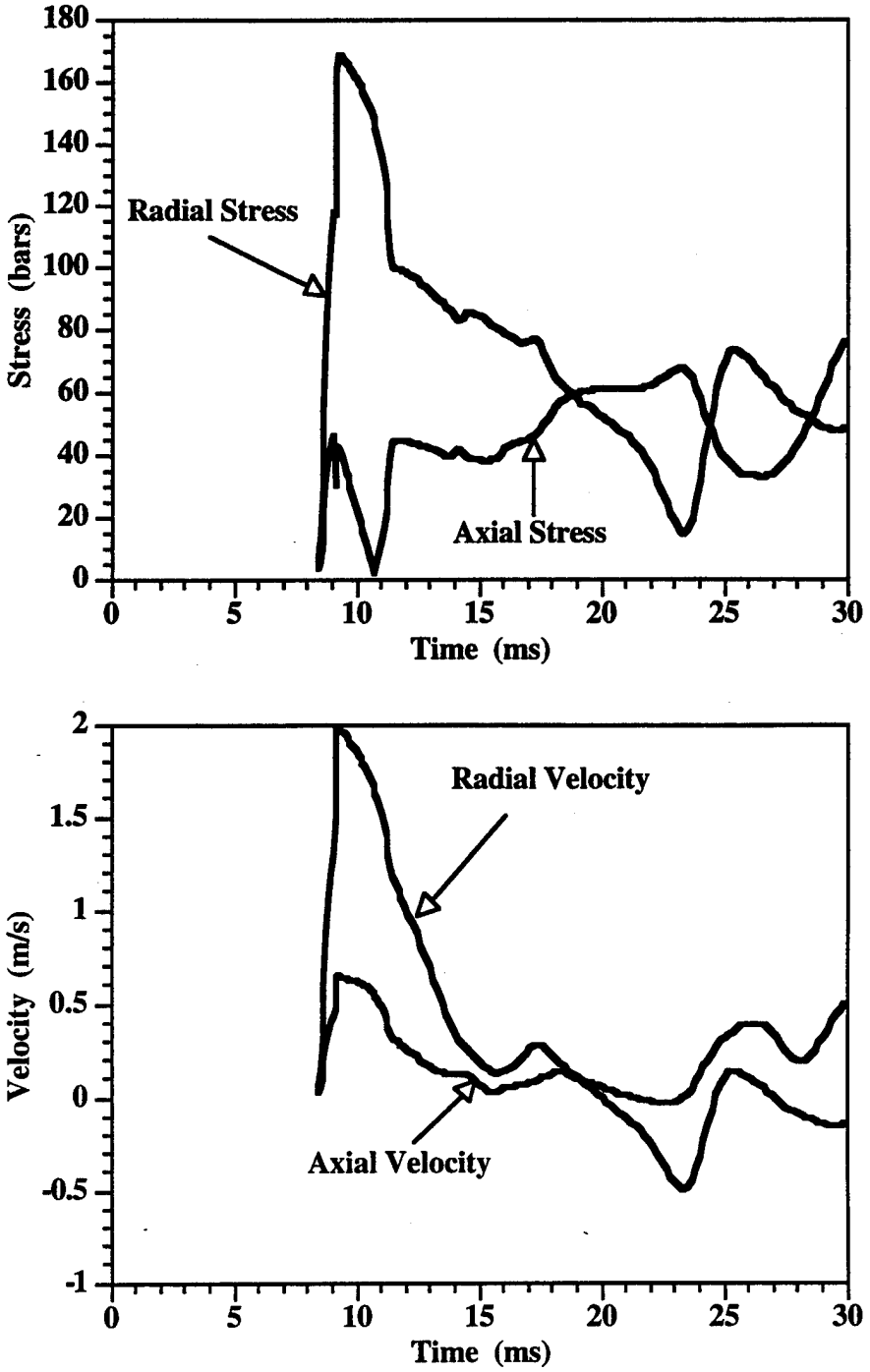

Figure 3-26. Stress and velocity histories for the SHIST calculation at 30 meters ground range and 30 meters depth.

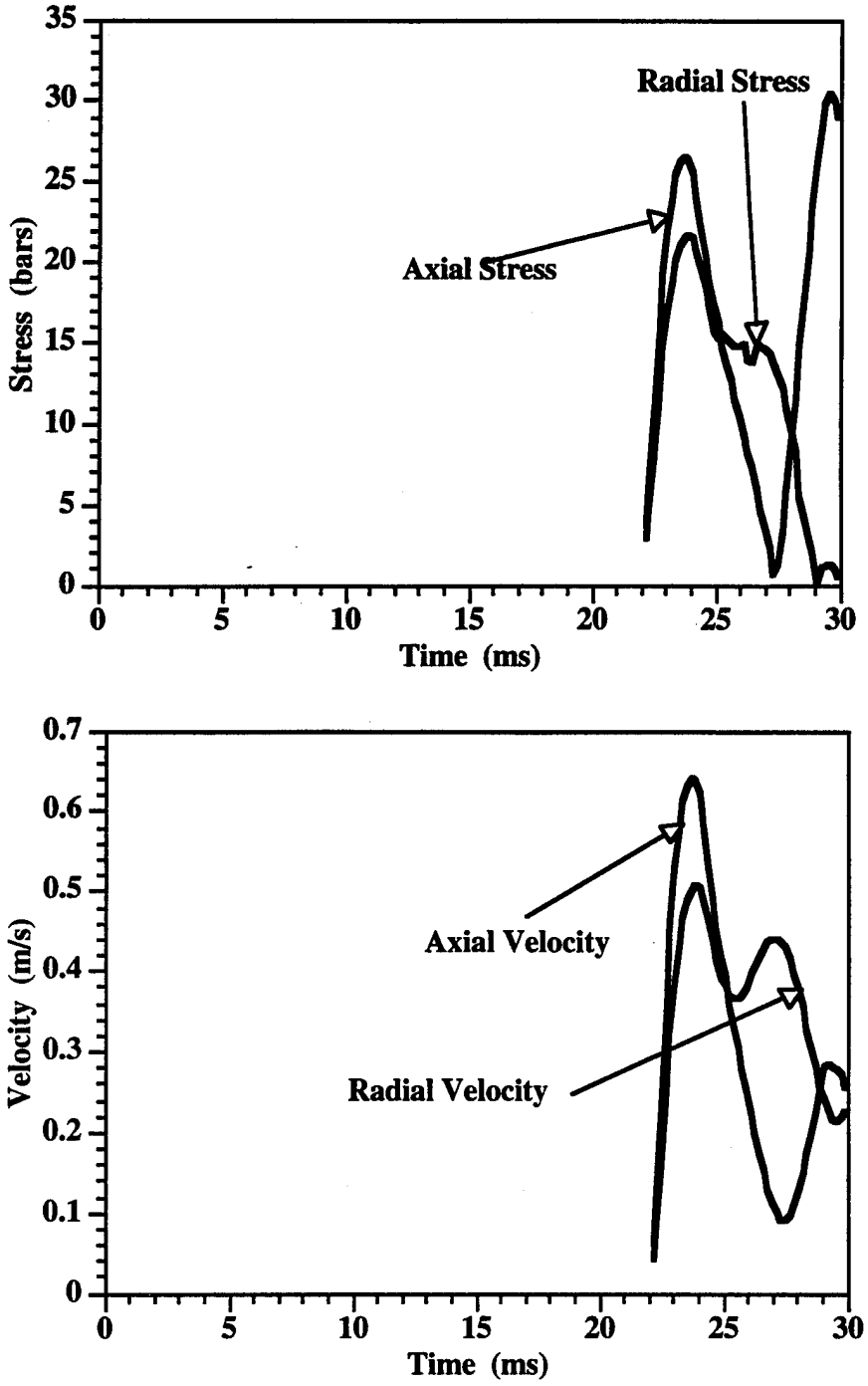

Figure 3-27. Stress and velocity histories for the SHIST calculation at 61 meters ground range and 5 meters depth.

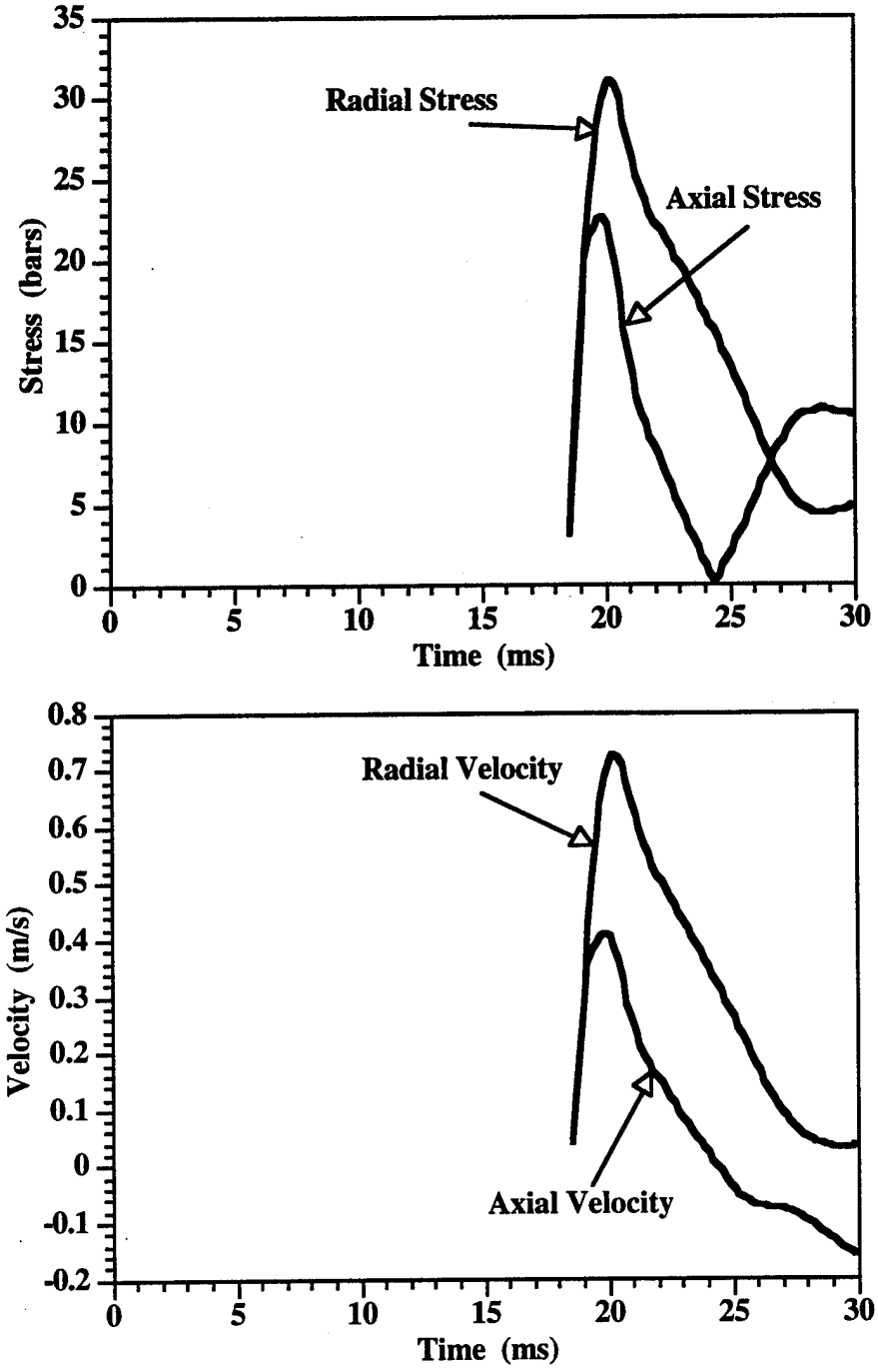

Figure 3-28. Stress and velocity histories for the SHIST calculation at 61 meters ground range and 15 meters depth.

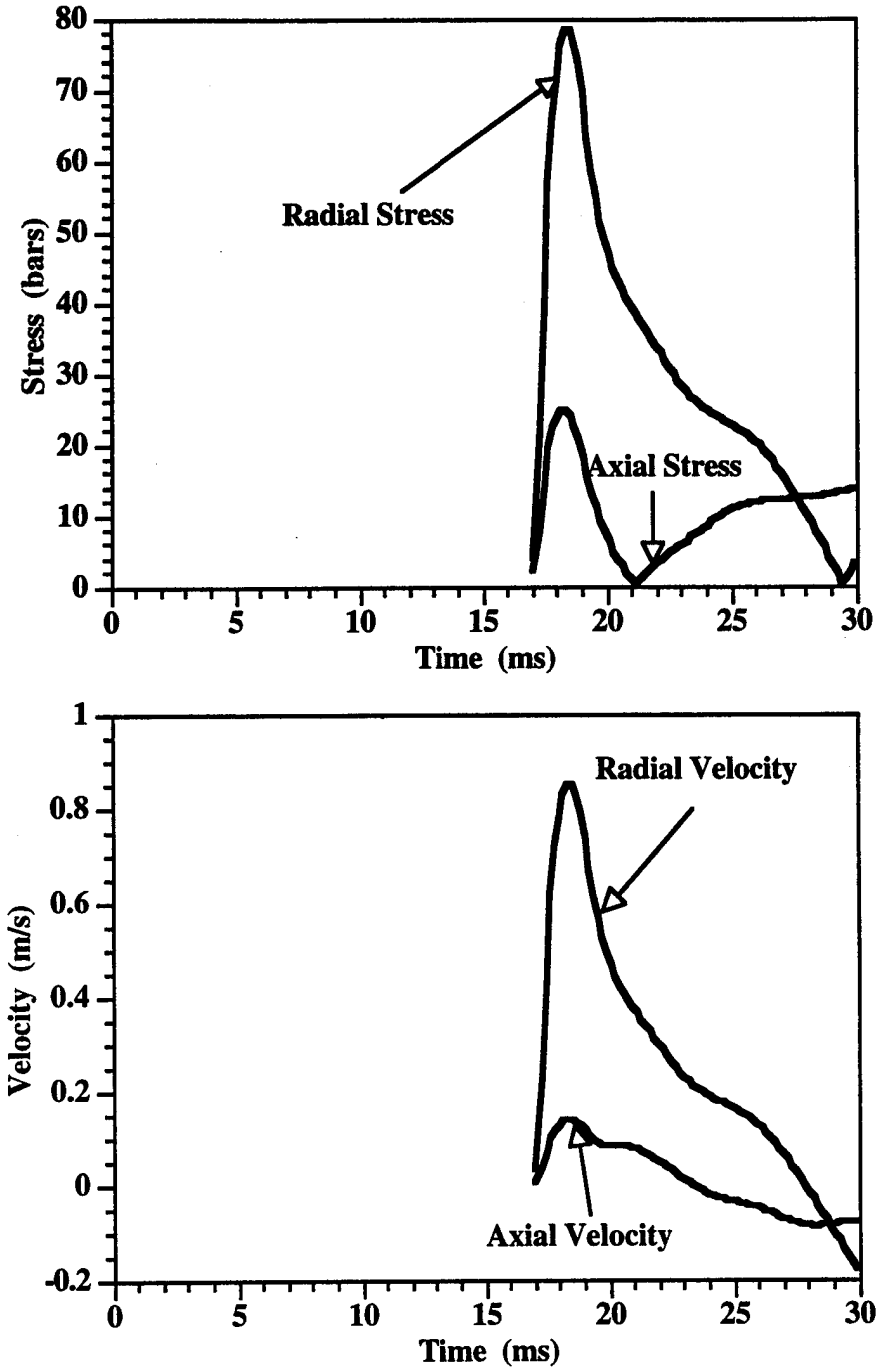

Figure 3-29. Stress and velocity histories for the SHIST calculation at 61 meters ground range and 30 meters depth.

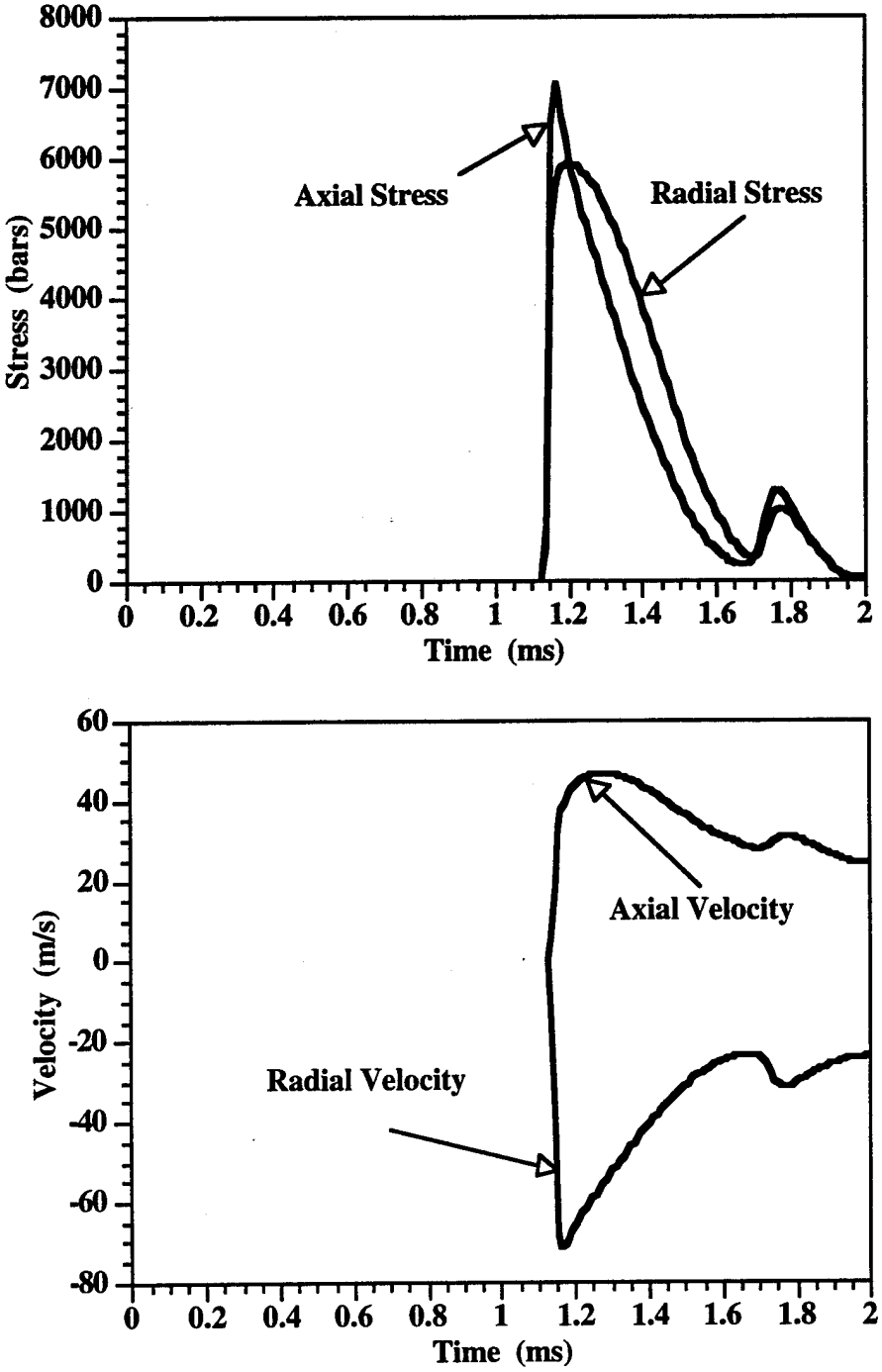

Figure 3-30. **Stress and velocity histories for the SHIST/DM4 calculation at 4 meters ground range and 5 meters depth.**

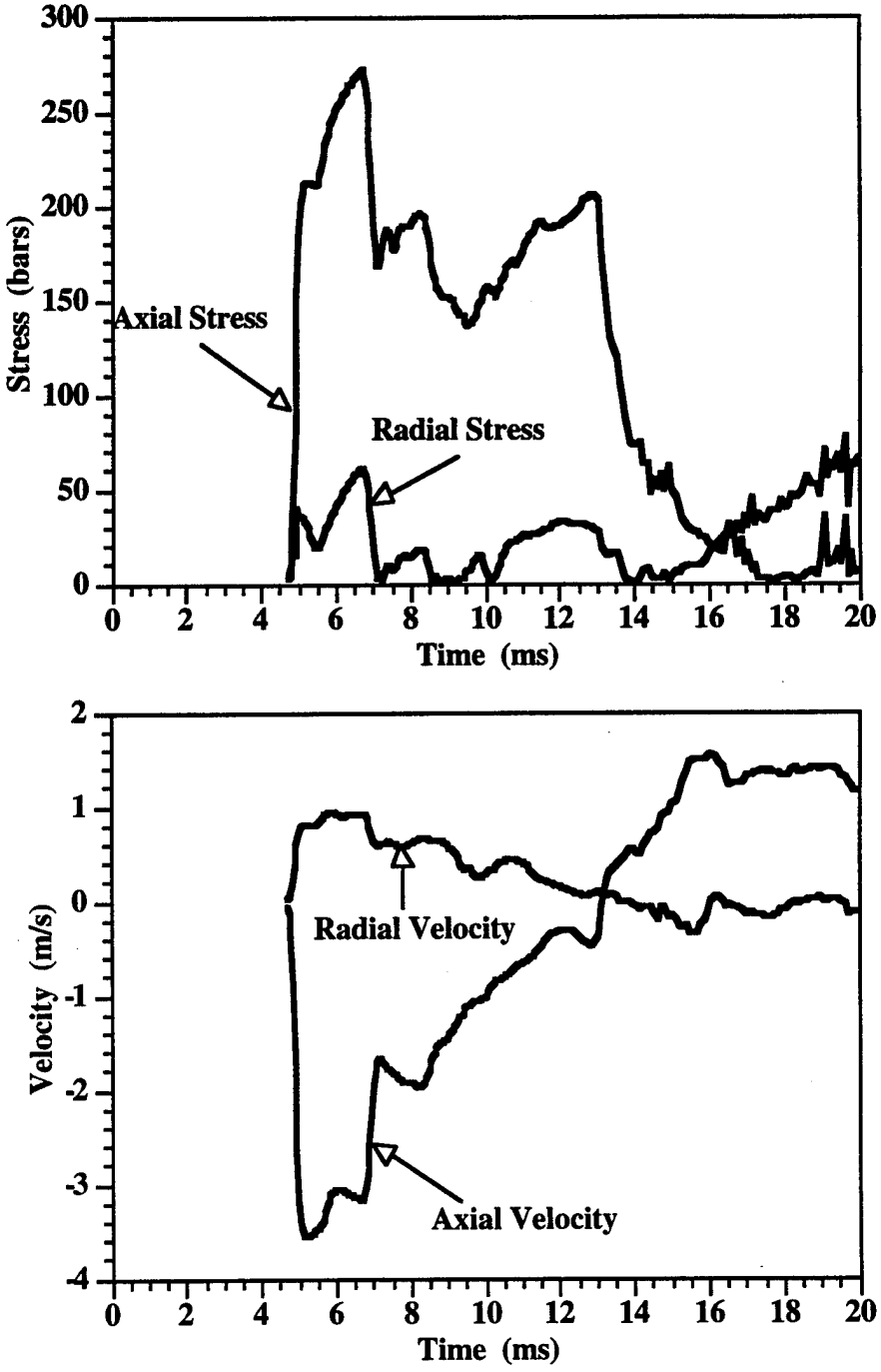

Figure 3-31. **Stress and velocity histories for the SHIST/DM4 calculation at 4 meters ground range and 15 meters depth.**

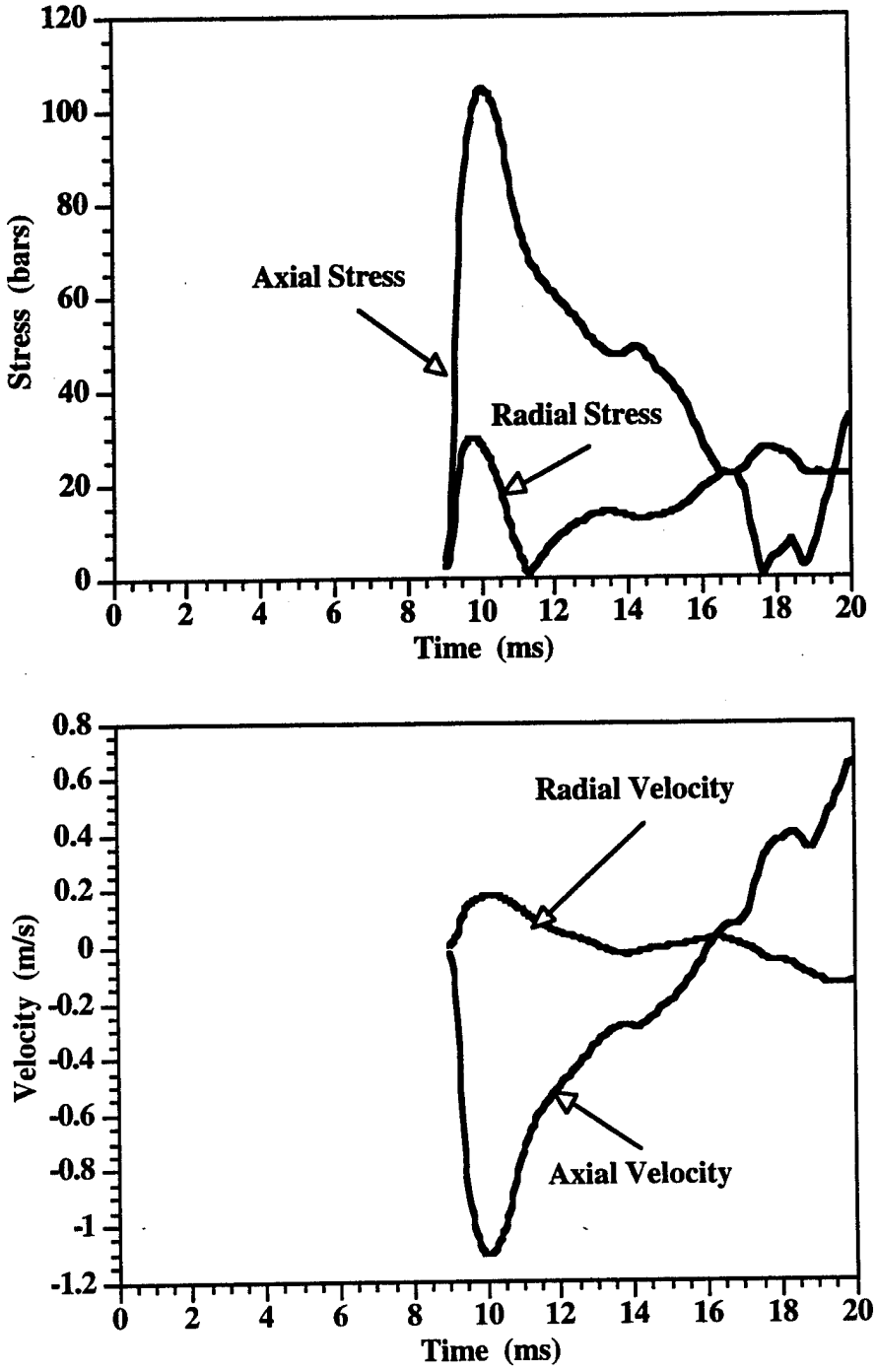

Figure 3-32. **Stress and velocity histories for the SHIST/DM4 calculation at 4 meters ground range and 30 meters depth.**

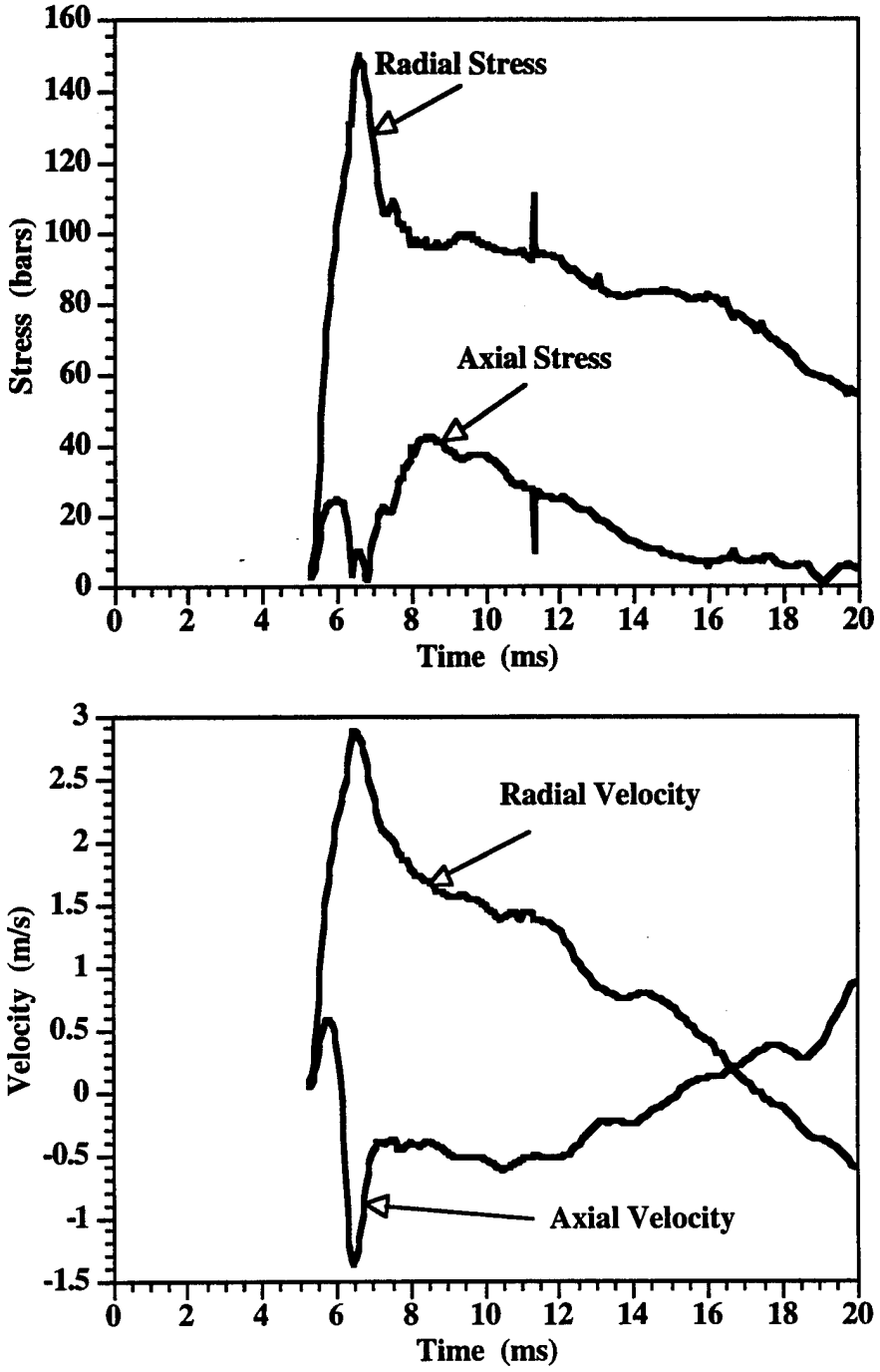

Figure 3-33. Stress and velocity histories for the SHIST/DM4 calculation at 15 meters ground range and 5 meters depth.

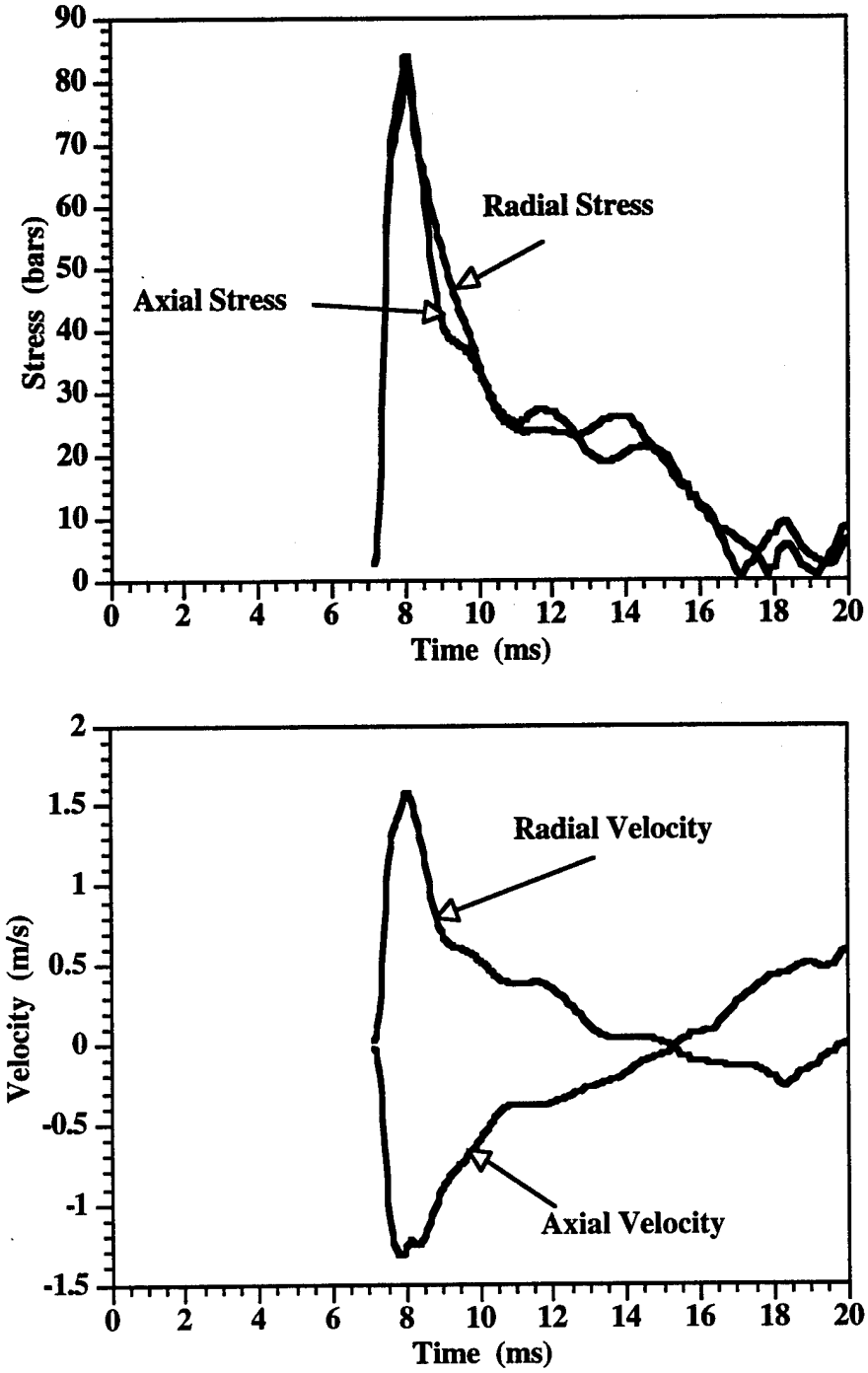

Figure 3-34. **Stress and velocity histories for the SHIST/DM4 calculation at 15 meters ground range and 15 meters depth.**

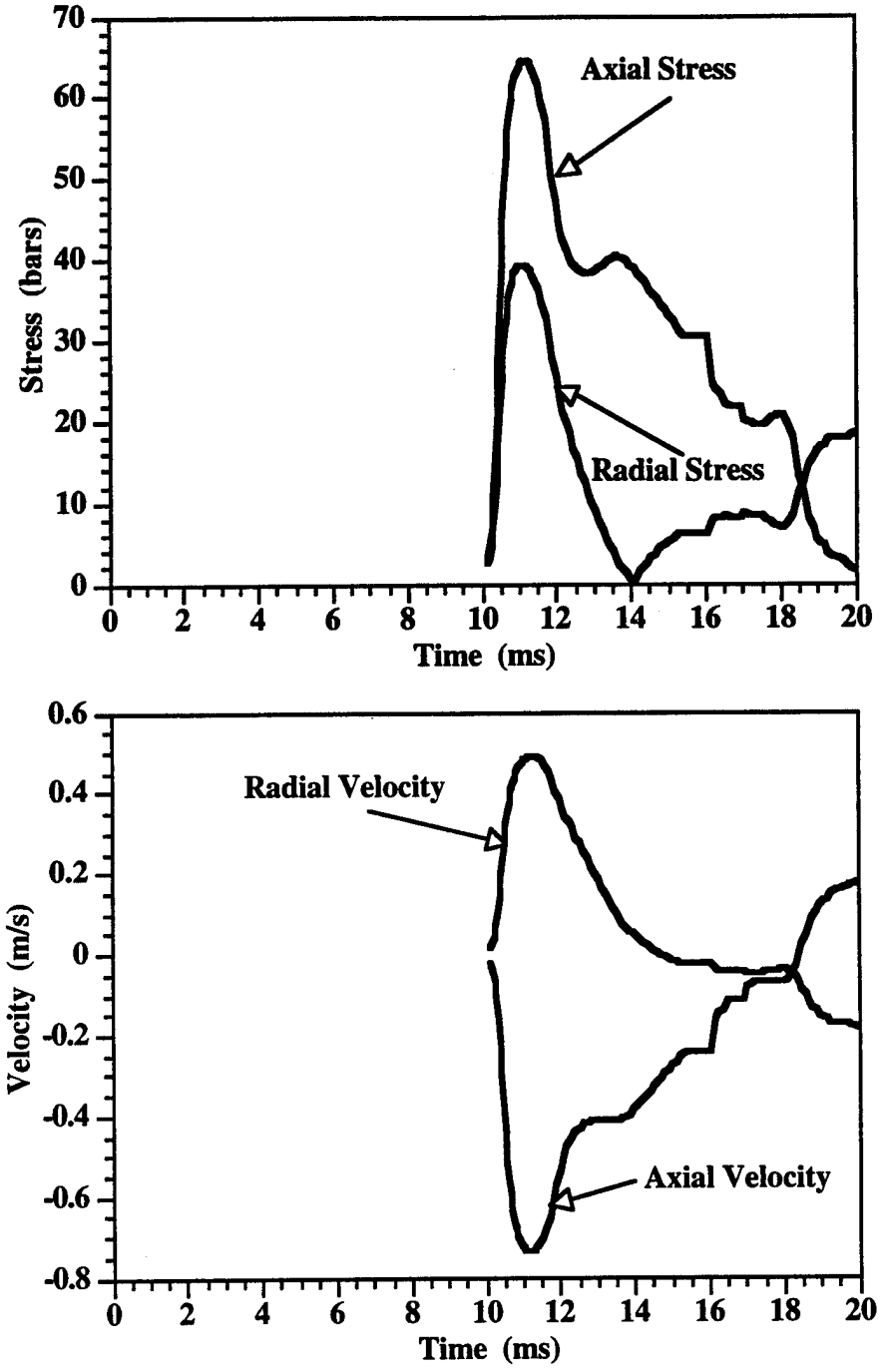

Figure 3-35. Stress and velocity histories for the SHIST/DM4 calculation at 15 meters ground range and 30 meters depth.

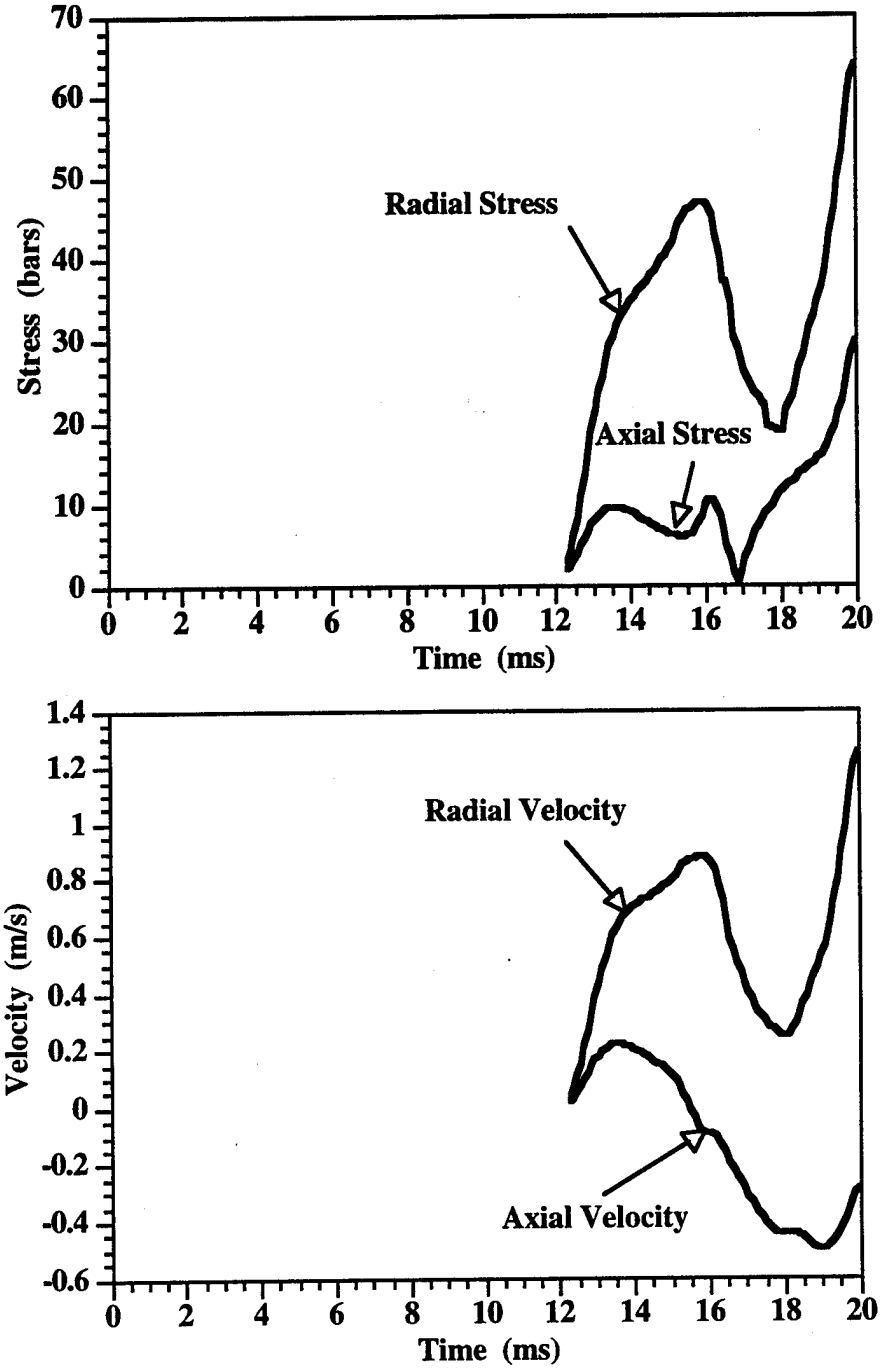

Figure 3-36. **Stress and velocity histories for the SHIST/DM4 calculation at 30 meters ground range and 5 meters depth.**

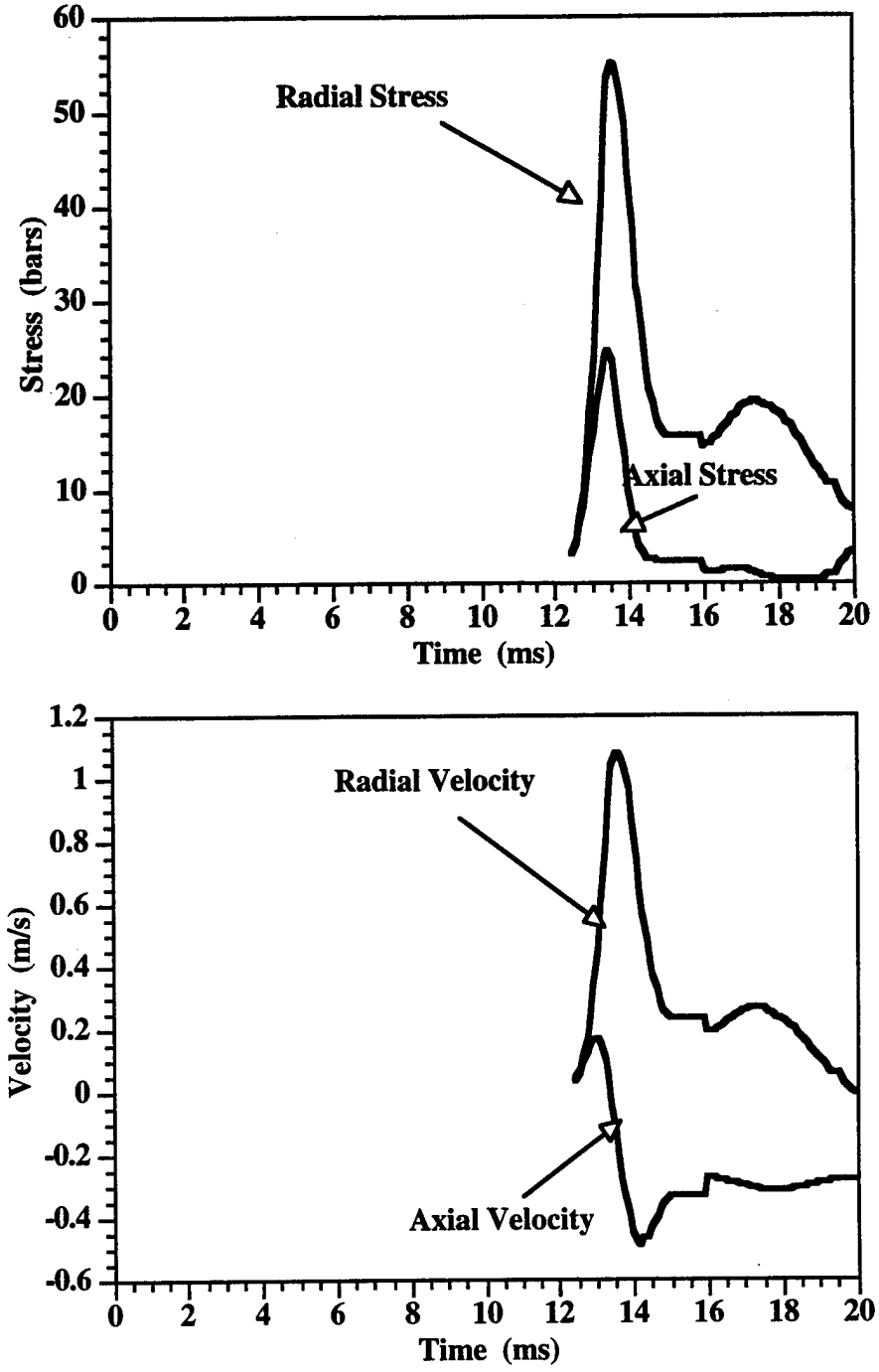

Figure 3-37. **Stress and velocity histories for the SHIST/DM4 calculation at 30 meters ground range and 15 meters depth.**

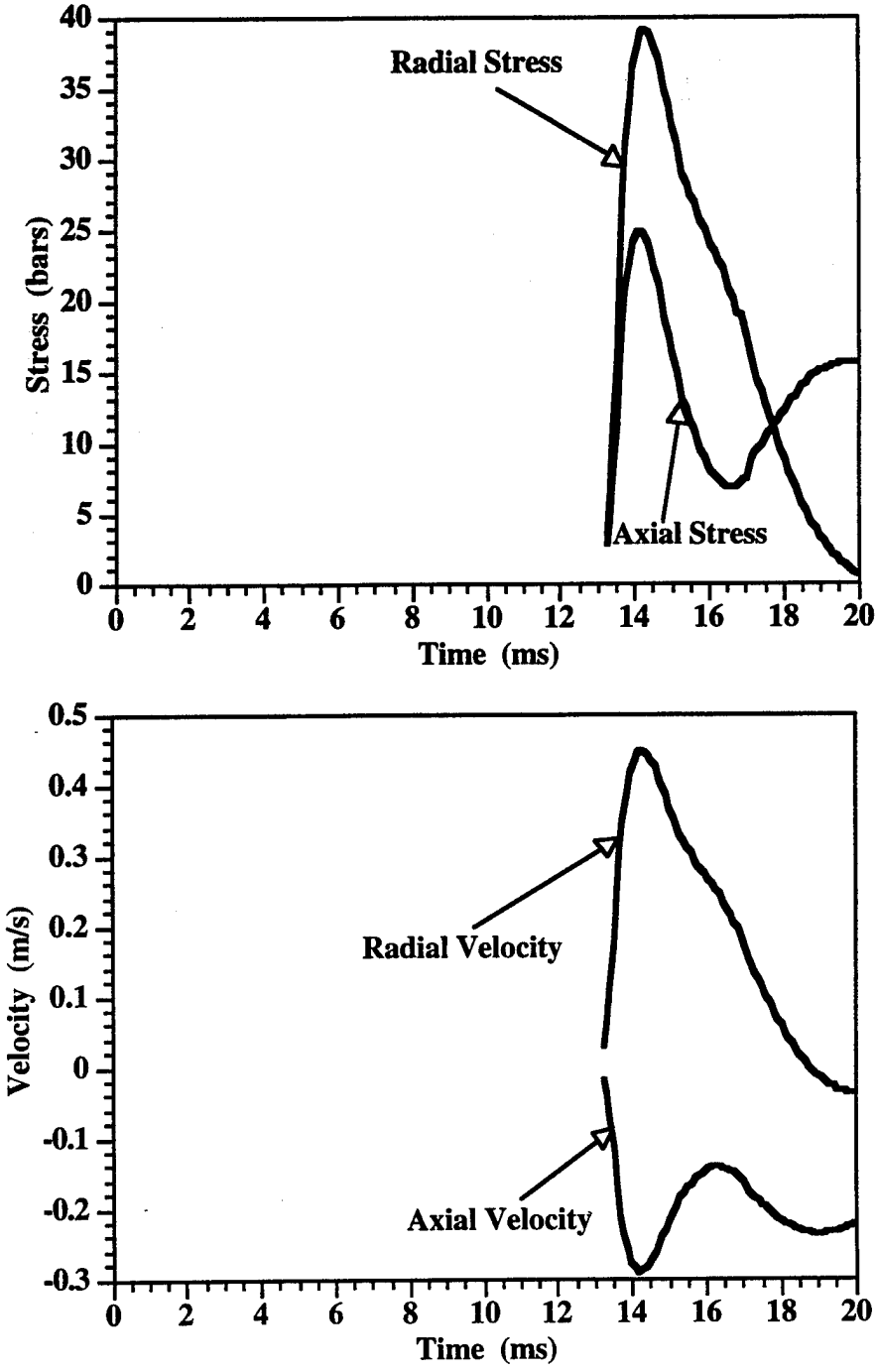

Figure 3-38. **Stress and velocity histories for the SHIST/DM4 calculation at 30 meters ground range and 30 meters depth.**

SECTION 4
CONCLUSIONS

In this report we have presented the results of two calculations done to predict ground motions for a proposed seismic source test in hard rock. The first provided ground motion predictions for the original design of the SHIST test while the second was intended to provide ground motion predictions to evaluate the possible use of the next DISTANT MOUNTAIN test, DM4, to satisfy some of the objectives of the SHIST test. Peak normal stress, peak velocity and ToA contours for these two calculations have been provided; these illustrate the similarities and difference between the two configurations. From the peak stress attenuation predictions directly below the two sources, we estimated an effective yield for the surface SHIST/DM4 configuration compared to the tamped SHIST configuration. The SHIST/DM4 effective yield was found to be approximately 17% of the SHIST yield. For the region calculated in these simulations, this effective yield applies only directly below the source; the equivalence does not apply to the near-surface region which is affected by the differences in the source locations and the fact that the near-surface layers do not scale. The 17% effective yield may be more applicable at larger ranges since the burial depth becomes a less important factor.

SECTION 5
REFERENCES

Allen, R. T., M. G. Lumsden, and J. E. Zerkle, "Water Shock Waves in Shallow Water," Defense Nuclear Agency, DNA-TR-93-112, 1993. (UNCLASSIFIED)

Cooper, C. H., and M. Biwer, "HYDROPLUS Verification Exercise on DISTANT ZENITH: Preliminary Results Report (U)," POR 7360, Field Command, Defense Nuclear Agency, November 1993. (CONFIDENTIAL-FORMERLY RESTRICTED DATA)

Dobratz, B. M., and P. C. Crawford, "LLNL Explosives Handbook: Properties of Chemical Explosives and Explosive Simulants," Lawrence Livermore National Laboratory, UCRL-52997 Change 2, January 1985. (UNCLASSIFIED)

Hermann, W., "Equation of State of Crushable Distended Materials," Sandia National Laboratories, SC-RR-66-2673, March 1968. (UNCLASSIFIED)

Martinez, A., Field Command, Defense Nuclear Agency, personal communication, July 1993. (UNCLASSIFIED)

McKay, M. W., R. N. Schlaug, T. L. Betlach, R. N. Byrne, and F. F. Y. Su, "Energy Coupling Studies," Defense Nuclear Agency, DNA-TR-93-47, October 1993. (UNCLASSIFIED)

Rinehart, E., Field Command, Defense Nuclear Agency, personal communication, August 1993. (UNCLASSIFIED)

Rocco, J. R., C. S. Sheffield, S. H. Schuster, D. W. Hatfield, A. V. Cooper, and J. M. Thompson, "DISTANT MOUNTAIN 1-3: Calculations, Charge Design, Prediction, and Analysis Report," Defense Nuclear Agency, POR 7519, August 1993. (UNCLASSIFIED)

Roessler, F. J., and B. Killian, "HYDROPLUS Verification Exercise on HUNTERS TROPHY: Preliminary Results Report (U)," POR 7511, Field Command, Defense Nuclear Agency, September 1993. (CONFIDENTIAL-FORMERLY RESTRICTED DATA)

DISTRIBUTION LIST

DNA-TR-94-150

DEPARTMENT OF DEFENSE

DEFENSE INTELLIGENCE AGENCY
ATTN: DT-1

DEFENSE NUCLEAR AGENCY
ATTN: DFSP
ATTN: DFTD D LINGER
ATTN: SPWE
ATTN: SPWE E TREMBA
2 CY ATTN: SSTL
ATTN: TDTV F RENSVOLD

DEFENSE TECHNICAL INFORMATION CENTER
ATTN: DTIC/OCP

FIELD COMMAND DEFENSE NUCLEAR AGENCY
ATTN: FCTN B HARRIS-WEST
ATTN: NVTV

FIELD COMMAND DEFENSE NUCLEAR AGENCY
ATTN: FCTT-T B RISTVET
ATTN: FCTT-T E RINEHART
ATTN: FCTT DR BALADI
ATTN: FCTT J HUGHES
ATTN: FCTTS J LEVERETTE
ATTN: FCTTS LT COL LEONARD
ATTN: FCTTS DR REINKE
ATTN: FCTTS P THOMPSON

DEPARTMENT OF THE ARMY

U S ARMY ENGR WATERWAYS EXPER STATION
ATTN: E JACKSON CEWES-SD-R
ATTN: J ZELASKO CEWES-SD-R

DEPARTMENT OF THE AIR FORCE

PHILLIPS LABORATORY
ATTN: PL/SUL

DEPARTMENT OF ENERGY

EG&G, INC
ATTN: D EILERS

LAWRENCE LIVERMORE NATIONAL LAB
ATTN: DONALD LARSON
ATTN: F HEUZE
ATTN: B DUNLAP
ATTN: LEWIS GLENN
ATTN: J RAMBO
ATTN: J WHITE
ATTN: W C MOSS
ATTN: R WARD
ATTN: TECH LIBRARY

LOS ALAMOS NATIONAL LABORATORY
ATTN: DAVID KING
ATTN: FRED APP
ATTN: T KUNKLE
ATTN: T MCKOWN
ATTN: J FRITZ
ATTN: C MORRIS
2 CY ATTN: REPORT LIBRARY
ATTN: J N JOHNSON
ATTN: THOMAS DEY
ATTN: TOM WEAVER

SANDIA NATIONAL LABORATORIES
ATTN: DIV 9321 W BOYER
ATTN: MIKE FURNISH
2 CY ATTN: TECH LIB 3141

DEPARTMENT OF DEFENSE CONTRACTORS

DEFENSE GROUP, INC
ATTN: ROBERT POLL

ENSCO INC
ATTN: P FISHER

JAYCOR
ATTN: CYRUS P KNOWLES

KAMAN SCIENCES CORP
ATTN: DASIAC

KAMAN SCIENCES CORPORATION
2 CY ATTN: DASIAC

KTECH CORP
ATTN: E SMITH
ATTN: FRANK DAVIES
ATTN: L LEE

LOGICON R & D ASSOCIATES
ATTN: J RENICK

MAXWELL LABORATORIES INC
ATTN: DR E PETERSON
ATTN: J BAKER
ATTN: J MORRIS
ATTN: P COLEMAN
ATTN: S PEYTON

SCIENCE APPLICATIONS INTL CORP
2 CY ATTN: D M O'DONNEL
ATTN: DAN PATCH
ATTN: JACK KLUMP
ATTN: L SCOTT
ATTN: MARTIN FOGEL
2 CY ATTN: M MCKAY

SRI INTERNATIONAL
ATTN: DR JIM GRAN
ATTN: MARK GROETHE
ATTN: P DE CARLI

TECH REPS, INC
ATTN: F MCMULLAN
ATTN: R NAEGELI

TERRA TEK, INC
ATTN: W MARTIN

TITAN CORPORATION (THE)
ATTN: A FREDERICKSON
ATTN: S SCHUSTER

DIRECTORY OF OTHER

MARYLAND UNIVERSITY OF
ATTN: RICHARD DICK